Linear and non-linear stability of floating viscous sheets

G. PFINGSTAG[1,2,3], B. AUDOLY[2] AND A. BOUDAOUD[3]

[1] Saint-Gobain Recherche, 39 Quai Lucien Lefranc, B.P. 135, 93303 Aubervilliers Cedex, France

[2]CNRS and UPMC Univ. Paris 06, UMR 7190, Institut Jean le Rond d'Alembert, Paris, France

[3]Laboratoire de Physique Statistique, Ecole Normale Supérieure, Université Pierre et Marie Curie, Université Paris Diderot, CNRS, 24 rue Lhomond, 75005 Paris, France

(Received Aug. 2010)

We study the stability of a thin, Newtonian viscous sheet floating on a bath of denser fluid. We first derive a general set of equations governing the evolution of a nearly flat sheet, accounting for geometrical nonlinearities associated with moderate rotations. We extend two classical models by considering arbitrary external body and surface forces; these two models follow from different scaling assumptions, and are derived in a unified way. The equations capture two modes of deformation, namely viscous bending and stretching, and describe the evolution of thickness, mid-surface and in-plane velocity as functions of two-dimensional coordinates. These general equations are applied to a floating viscous sheet, considering gravity, buoyancy and surface tension. We investigate the stability of the flat configuration when subjected to arbitrary in-plane strain. Two unstable modes can be found in the presence of compression. The first one combines undulations of the center-surface and modulations of the thickness, with a wavevector perpendicular to the direction of maximum applied compression. The second one is a buckling mode; it is purely undulatory and has a wavevector along the direction of maximum compression. A non-linear analysis yields the long-time evolution of the undulatory mode.

1. Introduction

When a longitudinal compressive force is applied to a thin, elastic rod, the rod remains straight below a well-defined critical force. Above this threshold, the rod bends. This instability known as buckling is also relevant to thin viscous threads and sheets. Buckling, and more generally, the dynamics viscous sheets have applications in both natural and industrial processes.

On geological time scales, the earth's crust can be modelled as a stack of superposed thin viscous sheets with different densities and viscosities that float on a denser mantle (Ramberg 1981). Lateral compression of such an assemblage generates phenomena like folding and mountain-building that can be understood as viscous buckling instabilities (Biot 1964; Johnson & Fletcher 1994; Perazzo & Gratton 2010). Thin viscous sheet models have also been used to model the large-scale deformation of continents (England & McKenzie 1983) and the buckling of oceanic lithosphere during subduction (Guillou-Frottier *et al.* 1995; Ribe *et al.* 2007).

On the time scales of organismal growth, cells and tissues can be considered as viscous bodies. For instance, the growth of plant cells was investigated using models of inflated anisotropic viscous shells (Dyson & Jensen 2010). At the supra-cellular level, a growing

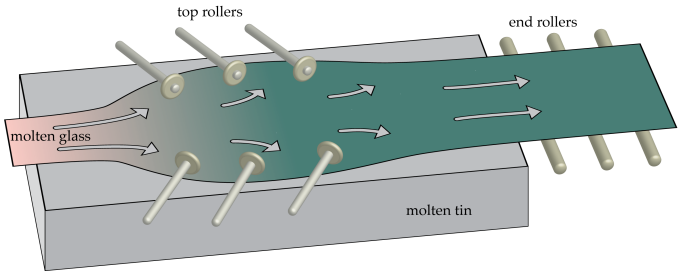

FIGURE 1. Principle of the float glass process: molten glass floats on top of molten tin. While it cools down, the glass is stretched by top rollers and end rollers to achieve the desired thickness. The float part is about 50 m long and 10 m wide.

tissue is compressed by neighbouring tissues with a lower growth rate. As a consequence, buckling instabilities can also be expected, yielding a mechanism for morphogenesis, as for organogenesis in plants (Steele 2000) or fingerprints formation (Kücken & Newell 2004), or the brain convolutions (Toro & Burnod 2005). We note however that, except in this last study, models were built upon purely elastic approaches.

In glass industry, thin sheets are given prescribed shapes and thickness by applying mechanical forcing while they cool down (Pearson 1985). In the second part of this paper, we will consider the case study of a floating sheet, which is motivated by both plate tectonics and glass industry. The glass float process (Pilkington 1969) is used for a continuous production of thin glass (Figure 1). At one end of a long bath of liquid tin, molten glass is poured from the furnace and spreads out forming a layer of floating glass (tin is denser than glass), cooling down as it gets farther from the furnace. In order to make the layer thinner than the capillary length, a set of rollers are used to stretch the floating sheet, which comes out solidified at the other end of the bath, after it has undergone a transverse compression. The corresponding compressive stress may induce buckling.

Taylor (1968) demonstrated the buckling of viscous threads and sheets in various experimental geometries. His work was inspired by the Rayleigh-Stokes analogy (Stokes 1845; Rayleigh 1896), according to which the Stokes equations for a viscous fluid are similar to the equations for the equilibrium of a Hookean (linearly elastic) incompressible solid, with the fluid velocity and viscosity replaced by the solid displacement and one-third the Young's modulus, respectively.

The seminal paper of Taylor (1968) inspired a number of subsequent studies. He first showed that a viscous thread can buckle under longitudinal compression, an instability that was investigated theoretically by Buckmaster *et al.* (1975) and Buckmaster & Nachman (1978). Taylor also repeated Barnes & Woodcock (1958)'s experiment on the coiling of a viscous jet impinging on a wall. In this geometry, buckling is triggered by the reaction force of the wall (see e.g. Cruickshank & Munson 1982; Mahadevan *et al.* 1998). These and other phenomena have been further investigated, and we refer the reader to Marheineke & Wegener (2009) for a review on viscous threads and jets.

Taylor (1968) also demonstrated buckling in a sheared annular layer of viscous liquid floating on an inviscid bath, and proposed a qualitative interpretation: shear stress induces compression at 45 degrees from the annulus midline. This experiment was repeated by Suleiman & Munson (1981) who investigated quantitatively the critical shear rate for buckling, and the wavelength of the undulations. They identified the relevant dimensionless groups but failed to predict the critical mode and its threshold. This problem was

again considered by Benjamin & Mullin (1988) who obtained a quantitative agreement with the experiments, based on a stability analysis of the 3D viscous flow. This instability is controlled by external forces (gravity and surface tension), and is essentially a buckling instability. An analysis based on the equations for thin viscous sheets was still lacking; one is proposed here as an application of our generic equations. A variant of the annular buckling experiment was proposed by Blake & Bejan (1984) who considered a rectangular floating sheet in contact with a container along three edges, and compressed along the fourth edge which is moving inwards.

The buckling of thin viscous sheets can also be induced by body forces. For instance, when an air bubble rising in a viscous liquid reaches the surface, a thin film of liquid separates it from ambient air. When this film is punctured, the air trapped in the bubble escapes; the hole grows while the viscous film falls under its own weight and makes wrinkles in the azimuthal direction (Debrégeas *et al.* 1998; Da Silveira *et al.* 2000). The same phenomenon occurs when a very viscous sheet drapes a stick (Boudaoud & Chaïeb 2001). In both cases, a semi-quantitative analysis taking advantage of the analogy between viscous and elastic sheets showed that gravity generates a compressive stress in the plane tangent to the sheet, while the most unstable mode is selected by a balance between gravity and viscous forces. Finally, the gravity-driven drawing of glass or polymer sheets can generate stress in the sheet and induce buckling (Filippov & Zheng 2010).

Most of the theoretical work on viscous sheets has relied on dimensional reduction. Indeed, asymptotic expansions in the limit of a small ratio between thickness and longitudinal length scale enable the derivation of governing equations for the dynamics of the mid-surface. Compared to the full, three-dimensional equations (e.g. Benjamin & Mullin 1988), dimensional reduction retains only the relevant modes of stretching and bending and can make more advanced analyses possible, like exploring the non-linear regime; it also eases numerical simulations. Dimensionally reduced models have been derived under specific assumptions: by Buckmaster *et al.* (1975); Ribe (2001) for two-dimensional problems (planar threads and cylindrical sheets); for axisymmetric three-dimensional problems where bending is dominated by stretching (Pearson & Petrie 1970*a*,*b*; Yarin *et al.* 1994); for non-axisymmetric, 3D problems where bending is dominated by stretching (van de Fliert *et al.* 1995), with applications to the drawing of a tube (Griffiths & Howell 2007, 2008, 2009) and of a flat sheet (Scheid *et al.* 2009; Filippov & Zheng 2010). Bending effects have only been considered by Howell (1996) in the case of nearly flat sheets and by Ribe (2002) for general shapes.

In this paper, we investigate the dynamics of nearly flat sheets. The closest work in the literature is that of Howell (1996) and Ribe (2002). Our approach is to derive the various limit models in a unified way, to consider arbitrary external forces (thereby extending Howell's results), and derive the equations in a form that is suited to stability analyses. Ribe considers finite rotations and the resulting equations are fairly general, except that external forces in the bulk are assumed to be constant. Our equations, being based on the small slope approximation, are compact and perfectly suited to the linear and non-linear stability analyses of floating viscous sheets. We use formal asymptotic expansions to deduce the equations for thin sheets from the equations for 3D viscous fluids, building on previous work done in the context of elastic plates such as the classical paper of Ciarlet (1980).

In Section 2 we derive two limit models depending on the magnitude of external loading. The full set of equations governing the thin sheet in 3D are given in Section 2.4. The analysis of stability of a floating sheet is prepared in Section 3: the general equations for thin viscous sheets are specified to the case of a floating sheet subjected to gravity, buoyancy and surface tension (§ 3.1); an unperturbed solution is defined (§ 3.2) and a lin-

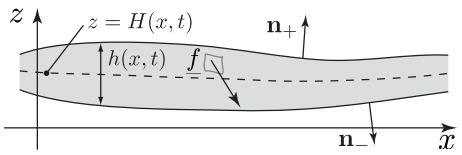

FIGURE 2. Cross-section of a viscous sheet in the plane (x, z) in a 2D geometry.

earization near this solution is introduced (§ 3.3). The linear stability of a floating sheet is investigated in Section 4 at short times, and in Section 5 at long times. An amplitude equation characterizing the non-linear buckling amplitude is derived in Section 4.2. In Section 6 we discuss the range of validity of our analysis and provide orders of magnitude relevant to applications.

2. Derivation of the models

We start by deriving a set of dimensionally reduced equations for thin viscous sheets, which are used in the stability analyses in the second part of the paper. In Section 2.1, we formulate the problem in two dimensions and introduce some useful notation. In Section 2.2, the equations for the balance of momentum in the fluid are expanded with respect to the small aspect ratio — thickness to typical longitudinal length — allowing integration across the thickness and yielding equilibrium equations for the stress resultants and torques at different orders. These equations of equilibrium are combined with the constitutive law for a Newtonian viscous fluid in Section 2.3. In Section 2.4, the assumption of a two-dimensional flow is relaxed. The reader not interested in the details can skip ahead to this last Section 2.4, where the equations governing the dynamics of viscous sheets subjected to external forces are summarized.

2.1. *Equilibrium equations in the 2D case*

Cartesian coordinates (x, y, z) are chosen such that the sheet lies in the (x, y) plane in undeformed state. We start with a two-dimensional formulation, assuming invariance with respect to the y-direction. At any time t, let $z = H(x, t)$ be the position of center surface of the sheet, and $h(x, t)$ its thickness. All variables, including forces, may depend on time; however this dependence shall be implicit to make notations more compact (the variable t is often omitted). The equations of the interfaces are

$$z_\pm(x, t) = H(x, t) \pm \frac{h(x, t)}{2}, \tag{2.1}$$

where the '+' is for the upper interface, and the '−' for the lower one. Let $\mathbf{n}_\pm(x)$ and $\mathbf{t}_\pm(x)$ denote the unit normals and tangents at either interface, with the orientation chosen as in figure 2. Both volume and surface forces may be applied on the sheet. These forces are collectively represented by a volume distribution of force $\mathbf{f}(x, z, t)$: surface forces such as surface tension are taken care of by a Dirac contribution to the volume force $\mathbf{f}$. We consider the limit of a small Reynolds number $\rho UL/\mu$ (μ being the fluid dynamic viscosity) and neglect inertial terms in the equations of equilibrium. Equilibrium in the

bulk and along the interfaces read, in terms of Cauchy stress tensor $\mathbf{S}$:

$$\boldsymbol{\nabla} \cdot \mathbf{S}(x,z) + \mathbf{f}(x,z) = \mathbf{0} \quad \text{for } z_-(x) \le z \le z_+(x) \tag{2.2a}$$

$$\mathbf{S}(x, z_\pm(x)) \cdot \mathbf{n}_\pm(x) = 0. \tag{2.2b}$$

Let us introduce some mathematical operators acting on a vertical slice of fluid. They shall help us keep compact notations while dealing with arbitrary distributions of forces across thickness. Given some function, $\phi(x,z)$, defined in the volume occupied by the sheet, we first define its thickness-integral, its first and second moments:

$$[I \cdot \phi](x) = \int_{z_-(x)}^{z_+(x)} \phi(x,z)\, \mathrm{d}z \tag{2.3a}$$

$$[J \cdot \phi](x) = \int_{z_-(x)}^{z_+(x)} (z - H(x))\, \phi(x,z)\, \mathrm{d}z \tag{2.3b}$$

$$[K \cdot \phi](x) = \int_{z_-(x)}^{z_+(x)} \frac{(z-H(x))^2}{2}\, \phi(x,z)\, \mathrm{d}z \tag{2.3c}$$

These operators will be useful for projecting the 3D forces into effective forces for the 2D model, see equations (2.30*a*) and (2.30*b*). In addition, the following two operators will be useful in the intermediate steps of the calculation:

$$[A \cdot \phi](x,z) = \int_{H(x)}^{z} \phi(x,z')\, \mathrm{d}z', \tag{2.3d}$$

$$[\chi \cdot \phi](x) = \int_{z_-(x)}^{z_+(x)} k_\chi(x,z)\, \phi(x,z)\, \mathrm{d}z, \tag{2.3e}$$

where the kernel is defined by

$$k_\chi(x,z) = \begin{cases} +1/2 & \text{if } H(x) < z < z_+(x) \\ -1/2 & \text{if } z_-(x) < z < H(x). \end{cases} \tag{2.3f}$$

Note that the result of all these operators is a function of the sole variable x, except for the 'indefinite' integral operator $[A \cdot \phi](x,z)$ which retains an additional dependence on the transverse coordinate z. The operators listed here satisfy useful identities derived in Appendix A.

2.2. *Expansion at different orders*

The model is derived by expansion with respect to the small aspect-ratio ϵ,

$$\epsilon = \frac{z^*}{L},$$

where z^* is the typical value of the sheet thickness $h(x)$, and L is a typical in-plane length. In-plane coordinate x is rescaled using L:

$$x = L\,\tilde{x}, \tag{2.4a}$$

where primes are used for rescaled variables. In contrast, the transverse coordinate z, thickness, and deflection of the center-surface $H(x)$ are rescaled using $z^* = \epsilon\, L$:

$$z = \epsilon\, L\, \tilde{z} \tag{2.4b}$$

$$h(x) = \epsilon\, L\, \tilde{h}(\tilde{x}) \tag{2.4c}$$

$$H(x) = \epsilon\, L\, \tilde{H}(\tilde{x}). \tag{2.4d}$$

The rescaled interface position $\tilde{z}_\pm(\tilde{x})$ is defined from equation (2.1) as $\tilde{z}_\pm(\tilde{x}) = \frac{1}{\epsilon L} z_\pm(x) = \tilde{H}(\tilde{x}) \pm \frac{\tilde{h}(\tilde{x})}{2}$. The upper and lower interfaces have small slope and the unit normal there read at order one in ϵ:

$$\mathbf{n}_\pm(\tilde{x}) = \begin{pmatrix} \mp\epsilon\, \tilde{z}_{\pm,\tilde{x}}(\tilde{x}) \\ \pm 1 \end{pmatrix}. \tag{2.5}$$

Here and elsewhere we use the notation $\phi_{,s} = \partial\phi/\partial s$ for the partial derivative of a function ϕ with respect to the variable s.

We consider the following rescaling and expansion for the internal stress $\mathbf{S}$

$$S_{xx}(x,z) = \frac{\mu\, U}{L}\left(\epsilon^0\, \tilde{S}^{(0)}_{xx}(\tilde{x},\tilde{z}) + \cdots\right), \tag{2.6a}$$

$$S_{xz}(x,z) = \frac{\mu\, U}{L}\left(\epsilon\, \tilde{S}^{(1)}_{xz}(\tilde{x},\tilde{z}) + \cdots\right), \tag{2.6b}$$

$$S_{zz}(x,z) = \frac{\mu\, U}{L}\left(\epsilon^0\, \tilde{S}^{(0)}_{zz}(\tilde{x},\tilde{z}) + \epsilon^2\, \tilde{S}^{(2)}_{zz}(\tilde{x},\tilde{z}) + \cdots\right), \tag{2.6c}$$

where ellipses denote higher-order terms. The overall factor $\mu\, U/L$ has been introduced by anticipating the viscous constitutive law, U being defined later as the typical in-plane velocity. For all terms but $\tilde{S}^{(0)}_{zz}$, the proposed hierarchy of powers of ϵ in the right-hand sides follows from a balance of the stress gradients $S_{ij,j}$ arising in the divergence in equation (2.2a); note that spatial derivatives scale differently along the in-plane and out-of-plane directions, namely $\partial/\partial x \sim \epsilon^0$ and $\partial/\partial z \sim 1/\epsilon$. The additional term $\tilde{S}^{(0)}_{zz}$ of order ϵ^0 is required because of the constitutive relation of the fluid. The pressure required to ensure incompressibility forces the orthogonal components S_{xx} and S_{zz} to have the same leading order with respect to ϵ, see equations (2.17a) and (2.28) — even if the fluid were compressible, the components S_{xx} and S_{zz} would still be coupled as both depend linearly on the components xx and yy of the strain rate tensor.

Substituting these scaling for the stress into the balance of forces (2.2a), we find that the net internal force $\boldsymbol{\nabla}\cdot\mathbf{S}$ is of order 1 along the x axis, and has contributions of order $1/\epsilon$ and ϵ along the z axis; consistency dictates the following scaling for the applied forces (density per unit volume):

$$f_x(x,z) = \frac{\mu\, U}{L^2}\left(\tilde{f}^{(0)}_x(\tilde{x},\tilde{z}) + \cdots\right) \tag{2.7a}$$

$$f_z(x,z) = \frac{\mu\, U}{L^2}\left(\frac{1}{\epsilon}\tilde{f}^{(-1)}_z(\tilde{x},\tilde{z}) + \epsilon\, \tilde{f}^{(1)}_z(\tilde{x},\tilde{z}) + \cdots\right). \tag{2.7b}$$

Here, f_x and f_z denote the projections of the force $\mathbf{f}$ onto the x and z directions: $\mathbf{f}(x,z) = \big(f_x(x,z), 0, f_z(x,z)\big)$. We have been led naturally to assume different scaling assumptions for the in-plane and out-of-plane components of the force in the presence of a slender geometry.

To avoid cumbersome notations, primes will be dropped in the remainder of this section: we shall always be dealing with rescaled quantities, unless specified otherwise.

We proceed to plug these expansions into the general equations for a 2D viscous fluid. Let us start with the equilibrium (2.2a), considered at order 0 along the x direction, and at orders both (-1) and 1 along the z direction:

$$S^{(0)}_{xx,x}(x,z) + S^{(1)}_{xz,z}(x,z) + f^{(0)}_x(x,z) = 0 \tag{2.8a}$$

$$S^{(0)}_{zz,z}(x,z) + f^{(-1)}_z(x,z) = 0 \tag{2.8b}$$

$$S^{(2)}_{zz,z}(x,z) + S^{(1)}_{xz,x}(x,z) + f^{(1)}_z(x,z) = 0. \tag{2.8c}$$

Regarding the consistency with respect to the parameter ϵ, recall that z is a first order quantity and so $\partial/\partial z$ is of order $1/\epsilon$; as a result, the term $S^{(1)}_{xz,z}$ for instance is of order $\epsilon/\epsilon = \epsilon^0$, and so is consistent with the other terms in the first equation.

Similarly, equation (2.2*b*) for the continuity of stress at the interfaces are spelled out at order 1 along the x direction, and at orders 0 and 2 along the z direction:

$$-z_{\pm,x}(x)\, S^{(0)}_{xx}(x, z_\pm(x)) + S^{(1)}_{xz}(x, z_\pm(x)) = 0 \tag{2.9a}$$

$$S^{(0)}_{zz}(x, z_\pm(x)) = 0 \tag{2.9b}$$

$$-z_{\pm,x}(x)\, S^{(1)}_{xz}(x, z_\pm(x)) + S^{(2)}_{zz}(x, z_\pm(x)) = 0. \tag{2.9c}$$

A solvability condition for $S^{(0)}_{zz}$ (also known as a Fredholm alternative) can be found by integrating the left-hand side of equation (2.8*b*) with respect to z and inserting the boundary conditions (2.9*b*) into $\int_{z_-}^{z_+} S^{(0)}_{zz,z}\,\mathrm{d}z = S^{(0)}_{zz}(x, z_+) - S^{(0)}_{zz}(x, z_-)$. This yields $\int_{z_-}^{z_+} f^{(-1)}_z\,\mathrm{d}z = 0$ or, in compact notation:

$$[I \cdot f^{(-1)}_z](x) = 0. \tag{2.10}$$

This equation implies a balance of transverse forces at dominant order, $f^{(-1)}_z$. An equation for the balance of transverse forces at second order, $f^{(1)}_z$, will be derived later by pushing the expansion farther, see equation (2.15).

The axial balance at first order is found by integration of equation (2.8*a*) with respect to z: $\left[I \cdot (S^{(0)}_{xx,x})\right] + \left[I \cdot (S^{(1)}_{xz,z})\right] + \left[I \cdot f^{(0)}_x\right] = 0$. Using the identities (A 1) and (A 2) derived in the Appendix A to rewrite the first and second term, we have

$$\left(\frac{\mathrm{d}[I \cdot S^{(0)}_{xx}]}{\mathrm{d}x} - (z_+)_{,x}\, S^{(0)+}_{xx} + (z_-)_{,x}\, S^{(0)-}_{xx}\right) + \left(S^{(1)}_{xz+} - S^{(1)}_{xz-}\right) + [I \cdot f^{(0)}_x] = 0,$$

where $S^{(i)\pm}_{\alpha\beta}$ is a short-hand notation for $S^{(i)}_{\alpha\beta}(x, z_\pm(x))$. By equation (2.9*a*), four terms cancel out in this equation and we have

$$N_{xx,x}(x) + [I \cdot f^{(0)}_x](x) = 0, \tag{2.11}$$

where we have introduced the membrane stress N_{ij}, also known as the internal stress resultant:

$$N_{ij}(x,t) = [I \cdot S^{(0)}_{ij}](x,t). \tag{2.12}$$

Equation (2.11) is a balance of longitudinal forces, the first term coming from internal stress, the second one from applied forces.

We push the expansion farther to obtain the transverse balance at the next order. Integration of equation (2.8*c*) with respect to z yields $\left[I \cdot (S^{(1)}_{xz,x})\right] + \left[I \cdot (S^{(2)}_{zz,z})\right] + \left[I \cdot f^{(1)}_z\right] = 0$. Repeating a similar calculation as that leading to equation (2.11) but using now the other boundary condition (2.9*c*), we end up with

$$[I \cdot S^{(1)}_{xz}]_{,x}(x) + [I \cdot f^{(1)}_z](x) = 0. \tag{2.13}$$

This equation still depends on a secondary quantity, $S^{(1)}_{xz}$, and needs more work.

To eliminate the shear stress $S^{(1)}_{xz}$, let us apply the moment operator J defined by equation (2.3*b*) on both sides of equation (2.8*a*):

$$[J \cdot (S^{(0)}_{xx,x})] + [J \cdot (S^{(1)}_{xz,z})] + [J \cdot f^{(0)}_x] = 0$$

The first term of this equation is rewritten using the identity (A 3) with $\gamma = S^{(0)}_{xx}$ (inte-

gration by parts along the x direction), and the second term using the other identity (A 4) with $\gamma = S^{(1)}_{xz}$ (integration by parts along the z direction). This yields

$$\Big([J\cdot S^{(0)}_{xx}]_{,x} + H_{,x}\,[I\cdot S^{(0)}_{xx}] - \frac{h(x)}{2}\,\Big(z_{+,x}\,S^{(0)+}_{xx} + z_{-,x}\,S^{(0)-}_{xx}\Big)\Big)\cdots \\ + \Big(-[I\cdot S^{(1)}_{xz}] + \frac{h(x)}{2}\,\Big(S^{(1)+}_{xz} + S^{(1)-}_{xz}\Big)\Big) + [J\cdot f^{(0)}_x] = 0.$$

By the boundary condition (2.9a), all terms proportional to $h(x)$ cancel out. Solving for the resultant of the shear stress, also known as the internal normal force, we find:

$$[I\cdot S^{(1)}_{xz}](x) = [J\cdot S^{(0)}_{xx}]_{,x}(x) + H_{,x}\,[I\cdot S^{(0)}_{xx}](x) + [J\cdot f^{(0)}_x](x). \tag{2.14}$$

Substituting this into equation (2.13), we finally obtain the balance of transverse forces at second order in compact form:

$$M_{xx,xx}(x) + (H_{,x}\,N_{xx})_{,x}(x) + [J\cdot f^{(0)}_x]_{,x}(x) + [I\cdot f^{(1)}_z](x) = 0, \tag{2.15}$$

where we have introduced the bending moment M_{ij}, defined by

$$M_{ij}(x,t) = [J\cdot S^{(0)}_{ij}](x,t). \tag{2.16}$$

Equation (2.15) complements the balance of transverse forces at dominant order 0, obtained earlier in equation (2.10). While the equation at dominant order was uncoupled to the dynamics of the sheet, the new equation (2.15) couples the viscous stress M_{xx} and N_{xx} to the applied force $f^{(0)}_x$ and $f^{(1)}_z$.

These equations are interpreted in Appendix B.

2.3. *Combining with viscous constitutive law*

The equations of equilibrium derived so far are valid for any thin sheet in the approximation of small slope. We shall now introduce the constitutive law for an incompressible, purely viscous Newtonian fluid with uniform dynamic viscosity μ — the case of thin sheets with non-uniform viscosity across thickness is considered in a different paper by the same authors (Pfingstag *et al.* 2011). Let $\mathbf{u}(x,z)$ be the velocity in the fluid. Conservation of volume and Stokes law read, returning temporarily to *non-scaled* variables:

$$\boldsymbol{\nabla}\cdot\mathbf{u}(x,z) = 0, \tag{2.17a}$$

$$\mathbf{S}(x,z) = -p(x,z)\,\mathbf{1} + 2\mu\,\mathbf{D}(x,z), \tag{2.17b}$$

where the strain rate tensor $\mathbf{D}(x,z)$ is the symmetric part of the gradient of velocity. The components of the velocity are noted

$$\mathbf{u}(x,z) = \big(u(x,z), 0, w(x,z)\big),$$

The second component along the y axis is set to zero since we assume a two-dimensional flow for the moment but this assumption will be relaxed later. There should be no confusion between the vector $\mathbf{u}$ and its x component, noted u.

At the interfaces, one more set of conditions involving the velocities is required in order to ensure kinematic compatibility:

$$w(x, z_\pm(x)) = z_{\pm,t}(x) + z_{\pm,x}(x)\,u(x, z_\pm(x)). \tag{2.18}$$

We consider additional scaling assumptions, which complement those given at the beginning of Section 2.2. We first use the constitutive law (2.17b) to rescale the pressure

and strain rate consistently with equation (2.6):

$$\mathbf{D}(x,z) = \frac{U}{L}\,\tilde{\mathbf{D}}(\tilde{x},z) \tag{2.19a}$$

$$p(x,y) = \frac{\mu U}{L}\tilde{p}(\tilde{x},\tilde{z}) \tag{2.19b}$$

We introduced earlier the quantity U, defined as the typical in-plane velocity: we shall therefore assume that the expansion for $u(x,z)$ starts like

$$u(x,z) = U\left(\tilde{u}^{(0)}(\tilde{x},\tilde{z}) + \cdots\right), \tag{2.19c}$$

where the ellipsis stands again for higher-order terms.

We also need to specify how time and transverse velocity scale with ϵ. Two different sets of scaling can be considered, as in the work of Howell (1996), namely the Trouton scaling and the BNT scaling. Here BNT stands for Buckmaster Nachman and Ting who first introduced this scaling (Buckmaster *et al.* 1975; Buckmaster & Nachman 1978). The Trouton scaling assumes $t \sim L/U$ and $w = \epsilon U$, while the BNT scaling assumes $t \sim \epsilon^2\, L/U$ and $w = \epsilon^{-1}\, U$. We recall here that since inertia has been neglected, time only appears in the kinematic equation (2.18) that describes the evolution of the sheet geometry. As will become apparent in the reduced equations for the sheet, the Trouton scaling is more elementary and corresponds to a deformation dominated by the stretching of the sheet, while the BNT scaling accounts for both stretching and bending. Both cases are taken care of by the notation

$$t = \epsilon^{2m}\,\frac{L}{U}\,\tilde{t}, \tag{2.20a}$$

$$w(x,z) = \epsilon^{1-2m}\,U\left(\tilde{w}^{(1-2m)}(\tilde{x},\tilde{z}) + \cdots\right). \tag{2.20b}$$

Value of the index m is defined to be 0 in Trouton case, and 1 in BNT case:

$$m = \begin{cases} 0 & \text{(Trouton)} \\ 1 & \text{(BNT)} \end{cases}, \qquad (1-m) = \begin{cases} 1 & \text{(Trouton)} \\ 0 & \text{(BNT)} \end{cases}. \tag{2.20c}$$

We shall use the 'reciprocal' indices m and $(1-m)$ routinely as a mean to track terms that are present with BNT scaling only, or with Trouton scaling only. Since m is only allowed to take on values 0 or 1, the following identity will be used later to simplify some expressions:

$$m\,(1-m) = 0. \tag{2.21}$$

In what follows, we shall again drop primes for the sake of readability: we deal implicitly with rescaled quantities, unless specified otherwise.

2.3.1. *Solving for the velocity field*

Let us consider the strain rate tensor $\mathbf{D}(x,z)$. The axial strain $D_{xx} = u^{(0)}_{,x}(x,z) + \ldots$ is a quantity of order ϵ^0 with our rescaling; transverse strain $D_{zz} = \epsilon^{-2m}\, w^{(1-2m)}_{,z}(x,z) + \ldots$ is a quantity of order ϵ^{-2m}, that is of order ϵ^0 in Trouton case ($m = 0$) and of order ϵ^{-2} in BNT case. In both cases, the incompressibility condition (2.17*a*) requires that the equation $D_{xx} + D_{zz} = 0$ holds at its leading order, ϵ^{-2m}: we have $w^{(1)}_{,z} + u^{(0)}_{,x} = 0$ in Trouton case, or $w^{(-1)}_{,z} = 0$ in BNT case. In compact notation, we have

$$w^{(1-2m)}_{,z}(x,z) + (1-m)\,u^{(0)}_{,x}(x,z) = 0. \tag{2.22a}$$

Consider now the shear strain rate, $D_{xy}(x,z) = \frac{1}{2}(u_{,z} + w_{,x})$. Its leading order, which

is formally ϵ^{-1} both in Trouton and BNT cases, has to cancel in order for the shear stress S_{xz} to remain of order ϵ as implied by equation (2.6b), and not ϵ^{-1}. The condition $u_{,z} + w_{,x} = 0$ yields $u^{(0)}_{,z} = 0$ in Trouton case, and $u^{(0)}_{,z} + w^{(-1)}_{,x} = 0$ in BNT case, which we summarize as

$$u^{(0)}_{,z}(x,z) + m\, w^{(1-2m)}_{,x}(x,z) = 0. \tag{2.22b}$$

Substitution of equation (2.22b) into the derivative of equation (2.22a) with respect to z yields, with the help of the identity (2.21): $w^{(1-2m)}_{,zz}(x,z) = 0$. A similar equation can be derived by substituting equation (2.22a) into the derivative of equation (2.22b) with respect to z. This yields

$$u^{(0)}_{,zz}(x,z) = 0, \qquad w^{(1-2m)}_{,zz}(x,z) = 0.$$

This implies that both $u^{(0)}(x,z)$ and $w^{(1-2m)}(x,z)$ depend linearly on z: for some functions $\overline{u}(x)$, $\overline{w}(x)$, $\breve{u}(x)$ and $\breve{w}(x)$ depending on x (and implicitly on time t) but not on z, we have

$$u^{(0)}(x,z) = \breve{u}(x)\,(z - H(x)) + \overline{u}(x),$$
$$w^{(1-2m)}(x,z) = \breve{w}(x)\,(z - H(x)) + \overline{w}(x).$$

The functions $\breve{u}(x)$ and $\breve{w}(x)$ can be found by substituting into equations (2.22): $\breve{u}(x) = -m\,\overline{w}_{,x}(x)$ and $\breve{w}(x) = -(1-m)\,\overline{u}_{,x}(x)$. We have just determined the leading orders of the axial and transverse velocities u and w, up to two functions $\overline{u}(x)$ and $\overline{w}(x)$ that do not depend on z:

$$u^{(0)}(x,z) = -m\,\overline{w}_{,x}(x)\,(z - H(x)) + \overline{u}(x) \tag{2.23a}$$
$$w^{(1-2m)}(x,z) = -(1-m)\,\overline{u}_{,x}(x)\,(z - H(x)) + \overline{w}(x). \tag{2.23b}$$

Let us now consider the kinematic compatibility condition (2.18), which we read off at its leading order ϵ^{1-2m}:

$$w^{(1-2m)}(x, z_\pm(x)) = z_{\pm,t}(x) + (1-m)\, z_{\pm,x}(x)\, u^{(0)}(x, z_\pm(x)).$$

Note that the last term, of order ϵ is not visible at the order $\epsilon^{1-2m} = \epsilon^{-1}$ when $m = 1$, but is visible at the order $\epsilon^{1-2m} = \epsilon$ when $m = 0$, hence the prefactor $(1-m)$. Inserting the definition of $z_\pm$ from equation (2.1) and the explicit form of $w^{(1-2m)}$ found in equation (2.23b), we have

$$-(1-m)\,\overline{u}_{,x}\left(\pm\frac{h}{2}\right) + \overline{w} = \left(H_{,t} \pm \frac{h_{,t}}{2}\right) + (1-m)\left(H_{,x} \pm \frac{h_{,x}}{2}\right)\overline{u}. \tag{2.24}$$

This equation has been simplified by dropping a term containing a factor $m(1-m)$, which is zero by equation (2.21). One condition holds on the upper interface (when replacing the symbol $\pm$ by $+$), and another condition holds on the lower interface (replacing $\pm$ by $-$). Considering the average of these two conditions (2.24), we find

$$\overline{w}(x) = H_{,t}(x) + (1-m)\, H_{,x}(x)\, \overline{u}(x).$$

When replaced into equation (2.23a), this yields an explicit solution for the in-plane velocity, after using equation (2.21) one more time:

$$u^{(0)}(x,z) = \overline{u}(x) - m\, H_{,xt}\,(z - H(x)). \tag{2.25}$$

In Trouton case ($m = 0$), the in-plane velocity $u^{(0)}$ appears to be independent of the transverse coordinate z; in BNT case, the last term shows up, accounting for the kinematics of bending.

Considering now the difference of equations (2.24) from the lower interface to the upper one, we find

$$-(1-m)\,\overline{u}_{,x}(x)\,h(x) = h_{,t} + (1-m)\,h_{,x}(x)\,\overline{u}(x),$$

which can be put in a more compact form:

$$h_{,t}(x) + (1-m)\,(h(x)\,\overline{u}(x))_{,x} = 0. \tag{2.26}$$

This is the conservation of volume integrated across the thickness: it reads $h_{,t}+(h\,\overline{u})_{,x}=0$ in Trouton case; in BNT case, we have simply $h_{,t}=0$.

2.3.2. *Solving for the in-plane stress*

Consider the equation (2.8b) for transverse equilibrium at order ϵ^{-1}, namely $S^{(0)}_{zz,z}(x,z)+f^{(-1)}_z(x,z)=0$. The general solution of this differential equation for $S^{(0)}_{zz}$ can be expressed in terms of the operator A carrying out z integration and of a constant of integration $\overline{S}_{zz}(x)$ independent of z:

$$S^{(0)}_{zz}(x,z) = -[A\cdot f^{(-1)}_z](x,z) + \overline{S}_{zz}(x).$$

Substituting this into equation (2.9b), which expresses transverse equilibrium of the interface at order ϵ^0, we find $\overline{S}_{zz}(x)=[A\cdot f^{(-1)}_z](x,z_+(x))$ and $\overline{S}_{zz}(x)=[A\cdot f^{(-1)}_z](x,z_-(x))$. Taking the average of these equalities, and using identity (A 5), we find the constant of integration $\overline{S}_{zz}(x)=[\chi\cdot f^{(-1)}_z](x)$. Therefore,

$$S^{(0)}_{zz}(x,z) = -[A\cdot f^{(-1)}_z](x,z) + [\chi\cdot f^{(-1)}_z](x). \tag{2.27}$$

Finally, the constitutive law (2.17b) yields $S^{(0)}_{xx}(x,z)=2\,u^{(0)}_{,x}(x,z)-p(x,z)$ and $S^{(0)}_{zz}(x,z)=-2\,u^{(0)}_{,x}(x,z)-p(x,z)$: by the condition of incompressibility, $D_{zz}=-D_{xx}=-u^{(0)}_{,x}$. Eliminating the pressure, we find

$$S^{(0)}_{xx}(x,z) = 4\,u^{(0)}_{,x}(x,z) + S^{(0)}_{zz}(x,z). \tag{2.28}$$

Substituting now our solution for $u^{(0)}(x,z)$ from equation (2.25), and our solution for $S^{(0)}_{zz}(x,z)$ from equation (2.27), we find an explicit solution for the in-plane stress:

$$S^{(0)}_{xx}(x,z) = 4\overline{u}_{,x}(x) - 4m\left(H_{,xt}(x)\,(z-H(x))\right)_{,x} - [A\cdot f^{(-1)}_z](x,z) + [\chi\cdot f^{(-1)}_z](x). \tag{2.29}$$

Again, note that the Trouton and BNT cases yields similar expressions, except for the bending term which is present only in BNT theory.

By integration of equation (2.29) across thickness we can now compute the stress resultant N_{ij} and moment M_{ij} defined earlier in equations (2.12) and (2.16). Using the identities (A 6a) and (A 6b) and the transverse equilibrium in equation (2.10) to simplify the terms proportional to $f^{(-1)}_z$, we have:

$$N_{xx}(x) = 4\,\mu\,h(x)\left(\overline{u}_{,x}(x) + m\,H_{,xt}(x)\,H_{,x}(x)\right) + [J\cdot f^{(-1)}_z](x), \tag{2.30a}$$

$$M_{xx}(x) = -m\,\frac{\mu\,h^3(x)}{3}H_{,xxt}(x) + [K\cdot f^{(-1)}_z](x). \tag{2.30b}$$

Note that the *transverse* force $f^{(-1)}_z$ appears in the expressions of the *longitudinal* stress resultant and moment; this contamination can be attributed to the coupling via the pressure. Even though its value is $\mu=1$ in our choice of rescaled units, we have restored the viscosity μ in the above equations for improved readability.

2.4. *Generalization to 3D*

We recapitulate all the equations that govern the dynamics of the viscous sheet, which have been obtained previously by expansion. In passing, we relax the assumption of invariance along the y direction (3D case); we shall not justify again the derivation of the 3D setting as it goes along the same lines as the 2D setting. The in-plane variables are now x and y; the in-plane components of the external force are noted $(f_x(x,y,z), f_y(x,y,z))$. We describe the evolution of the thickness $h(x,y,t)$ and height $H(x,y,t)$ of the sheet, and the in-plane average velocity $(\overline{u}(x,y,t), \overline{v}(x,y,t))$. As earlier, the Trouton and BNT models are gathered in a single set of equations, by introducing two indices $(1-m)$ and m: the Trouton model is recovered by setting $(1-m)=1$ and $m=0$, and the BNT model by $(1-m)=0$, $m=1$.

The following set of equations extends the equations of the previous section. Mass conservation (2.26) becomes:

$$h_{,t}(x,y) + (1-m)\left(\frac{\partial(\overline{u}(x,y)\,h(x,y))}{\partial x} + \frac{\partial(\overline{v}(x,y)\,h(x,y))}{\partial y}\right) = 0. \tag{2.31}$$

The axial force balance (2.11) now reads:

$$\left\{\begin{array}{l} N_{xx,x}(x,y) + N_{xy,y}(x,y) = -[I\cdot f_x^{(0)}](x,y) \\ N_{xy,x}(x,y) + N_{yy,y}(x,y) = -[I\cdot f_y^{(0)}](x,y). \end{array}\right. \tag{2.32}$$

The transverse balance of force at order 0 reads, from equations (2.10):

$$[I\cdot f_z^{(-1)}] = 0, \tag{2.33a}$$

and order 2, from equation (2.15):

$$\begin{aligned} &\big(M_{xx,xx} + 2M_{xy,xy} + M_{yy,yy}\big) + \big(N_{xx}\,H_{,xx} + 2N_{xy}\,H_{,xy} + N_{yy}\,H_{,yy}\big) \\ &\quad + \big(-H_{,x}\,[I\cdot f_x^{(0)}] - H_{,y}\,[I\cdot f_y^{(0)}] + [J\cdot f_x^{(0)}]_{,x} + [J\cdot f_y^{(0)}]_{,y}\big) + [I\cdot f_z^{(1)}] = 0. \end{aligned} \tag{2.33b}$$

Note that we have expanded the derivative in the second term in equation (2.15) here, and simplified using the in-plane equilibrium. The membrane stress N_{ij} and the internal moment M_{ij} are given by effective constitutive laws, which extend those given in equations (2.30):

$$\left\{\begin{array}{rcl} N_{xx}(x,y) &=& 2\mu\,h(x,y)\big(2(\overline{u}_{,x}(x,y) + m\,H_{,xt}\,H_{,x}) + (\overline{v}_{,y}(x,y) + m\,H_{,yt}\,H_{,y})\big) \\ && +[J\cdot f_z^{(-1)}](x,y) \\ N_{xy}(x,y) &=& \mu\,h(x,y)\big((\overline{u}_{,y}(x,y) + m\,H_{,xt}\,H_{,y}) + (\overline{v}_{,x}(x,y) + m\,H_{,yt}\,H_{,x})\big) \\ N_{yy}(x,y) &=& 2\mu\,h(x,y)\big((\overline{u}_{,x}(x,y) + m\,H_{,xt}\,H_{,x}) + 2(\overline{v}_{,y}(x,y) + m\,H_{,yt}\,H_{,y})\big) \\ && +[J\cdot f_z^{(-1)}](x,y), \end{array}\right. \tag{2.34}$$

$$\left\{\begin{array}{rcl} M_{xx}(x,y) &=& -m\,\dfrac{\mu\,h^3(x,y)}{3}\,\big(H_{,xxt} + \tfrac{1}{2}\,H_{,yyt}\big) + [K\cdot f_z^{(-1)}](x,y) \\ M_{xy}(x,y) &=& -m\,\dfrac{\mu\,h^3(x,y)}{3}\,\big(\tfrac{1}{2}\,H_{,xyt}\big) \\ M_{yy}(x,y) &=& -m\,\dfrac{\mu\,h^3(x,y)}{3}\,\big(H_{,yyt} + \tfrac{1}{2}\,H_{,yyt}\big) + [K\cdot f_z^{(-1)}](x,y). \end{array}\right. \tag{2.35}$$

Here the mean surface position H is a function of x, y and t. Equations (2.34) and (2.35) are written in compact form and justified in full detail in a follow-up paper by the same authors (Pfingstag *et al.* 2011).

2.5. *Discussion*

These equations generalize the results of Howell (1996) to arbitrary forces. The general equations of Ribe (2002) can be shown to be equivalent to the compact set of equations above in the case of small slope and constant bulk external forces. The order of magnitude of the transverse forces and the scaling for the time should now be chosen depending on the specific problem considered. Note that the order of magnitude U of the in-plane velocity can be set by the forcing applied along the boundaries, or by distributed in-plane forces f_x and f_y.

When transverse forces f_z are large compared to $\mu\, U/L^2$, they should be considered to be of order (-1) and assigned to the contribution $f_z^{(-1)}$; then the transverse balance is given by equation (2.33a), and equation (2.33b) can be discarded. In that case, the BNT scaling suppresses all time derivatives, indicating that the time scale considered is too short for the sheet to evolve. By contrast, the Trouton scaling corresponds to observing the sheet over a much longer time scale, where it does evolve. In such circumstances, Trouton scaling is appropriate and BNT scaling can be viewed as a degenerate case.

By contrast, when transverse forces f_z are small compared to $\mu\, U/L^2$, one should set $f_z^{(-1)} = 0$, assign them to $f_z^{(1)}$ and use equation (2.33b) for the transverse balance of forces. Combined with Trouton scaling, this equation is singular in the presence of compressive stress: equation (2.33b) attempts to describe buckling but with a zero bending stiffness: with $m = 0$ in equation (2.35), the bending rigidity appears to be zero in Trouton case. This leads to spatial undulations with arbitrarily small wavelength, a phenomenon known as membrane wrinkling in the context of elastic plates and shells, see e.g. the work of Dret & Raoult (1995). Therefore in the case of 'small' transverse forces, BNT scaling is more appropriate.

Note that we can combine the Trouton and BNT models into a single, hybrid model. The trick is (i) to re-sum, *i.e.* write the equations for $f_z = \epsilon^{-1}\, f_z^{(-1)} + \epsilon\, f_z^{(1)} + \cdots$ and not for $f_z^{(-1)}$ and , $f_z^{(1)}$ separately: this has the effect of removing ϵ from the equations and there is no longer need to keep track of the indices in parentheses for the order; (ii) to retain *all* terms that appear either in the Trouton or BNT model; we take $m = 0$ in (2.31):

$$h_{,t}(x,y) + \frac{\partial(\overline{u}(x,y)\, h(x,y))}{\partial x} + \frac{\partial(\overline{v}(x,y)\, h(x,y))}{\partial y} = 0, \tag{2.36}$$

$m = 1$ in the stress resultants (2.34) and moments (2.35):

$$\left\{\begin{array}{rcl} N_{xx}(x,y) & = & 2\mu\, h(x,y)\left(2(\overline{u}_{,x}(x,y) + H_{,xt}\, H_{,x}) + (\overline{v}_{,y}(x,y) + H_{,yt}\, H_{,y})\right) \\ & & +[J \cdot f_z^{(-1)}](x,y) \\ N_{xy}(x,y) & = & \mu\, h(x,y)\left((\overline{u}_{,y}(x,y) + H_{,xt}\, H_{,y}) + (\overline{v}_{,x}(x,y) + H_{,yt}\, H_{,x})\right) \\ N_{yy}(x,y) & = & 2\mu\, h(x,y)\left((\overline{u}_{,x}(x,y) + H_{,xt}\, H_{,x}) + 2(\overline{v}_{,y}(x,y) + H_{,yt}\, H_{,y})\right) \\ & & +[J \cdot f_z^{(-1)}](x,y), \end{array}\right. \tag{2.37}$$

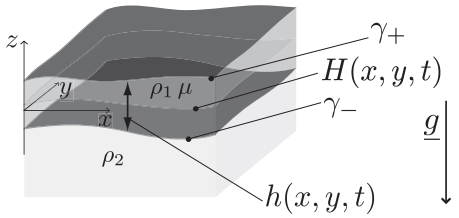

FIGURE 3. Geometry of a floating viscous sheet in a 3D geometry.

$$\left\{\begin{array}{rcl} M_{xx}(x,y) &=& -\dfrac{\mu\,h^3(x,y)}{3}\,\left(H_{,xxt}+\frac{1}{2}\,H_{,yyt}\right)+[K\cdot f_z^{(-1)}](x,y)\\[2ex] M_{xy}(x,y) &=& -\dfrac{\mu\,h^3(x,y)}{3}\,\left(\frac{1}{2}\,H_{,xyt}\right)\\[2ex] M_{yy}(x,y) &=& -\dfrac{\mu\,h^3(x,y)}{3}\,\left(H_{,yyt}+\frac{1}{2}\,H_{,yyt}\right)+[K\cdot f_z^{(-1)}](x,y). \end{array}\right. \tag{2.38}$$

Then, the problem is governed by mass conservation (2.36), longitudinal force balance (2.32) and transverse force balance (2.33*b*), complemented with the stress resultants (2.37) and moments (2.38). The resulting hybrid model enjoys the following property: it boils down to either the Trouton or BNT model when the corresponding scaling assumptions are made. As such, it provides a formal unification of the two models which can be convenient *e.g.* to set up numerical simulations.

3. Application to the stability of floating viscous sheets

3.1. *Case of a floating, 3D sheet with gravity, buoyancy and surface tension*

In the remainder of this paper, we apply our equations to a specific geometry: a thin, viscous sheet floating on a bath at hydrostatic equilibrium, with surface tension at the lower and upper interfaces. Each of the surface tensions γ_+ and γ_- at the upper and lower interfaces are assumed to be uniform. An in-plane flow of typical velocity U is imposed in the sheet, e.g. through in-plane loading. The density of the sheet material ρ_1 is smaller than that of the bath ρ_2. Let $z = H^b$ be the height of the free surface of the bath when the sheet is absent. The bath is an inviscid fluid at rest; the pressure in the bath is purely hydrostatic, $p = \rho_2\,g\,(H^b - z)$, where g is the acceleration of gravity.

The weight per unit volume of the sheet is simply $(\rho_1\,g)$. Let z^* be the typical vertical displacement of the interfaces, be it due to deformations of the initially planar mid-surface, or to variations of thickness. Surface forces applied at the interfaces come from hydrostatic pressure, of order $(\rho_2\,g\,z^*)$, and capillary pressure, of order $(\gamma\,z^*/L^2)$. Here γ is the typical value of surface tension and L an characteristic in-plane length, such as the wrinkling wavelength, or a scale imposed by the in-plane flow. These surface forces can be compared to the typical viscous force per unit volume, $(\mu\,U/L^2)$, times the typical thickness z^*, using nondimensional numbers. Jeffreys number (Jeffreys 1925; O'Keefe

1969) compares gravity and viscosity,

$$\mathrm{Je} = \frac{\rho\, g\, L^2}{\mu\, U}, \tag{3.1}$$

where ρ stands for the order of magnitude of any of the densities. Similarly, the inverse capillary number compares surface tension and viscosity

$$1/\mathrm{Ca} = \frac{\gamma}{\mu\, U}. \tag{3.2}$$

A number of models could be considered based on these ingredients. We focus here on the case where gravity and surface tension both need to be considered in addition to viscosity. This is the most interesting situation since we have two factors that can limit the instabilities and which are potentially in competition: one relevant to large wavelengths and the other one to small wavelengths. Specifically, we consider two cases:

(*a*) Both the Jeffreys Je and inverse capillary 1/Ca number are small; transverse forces should be considered of order ϵ. The argument of Section 2.5 suggests that we then consider short times and use the BNT scaling. The expressions of the applied forces read

$$\begin{aligned}
f_z^{(-1)} &= 0 \\
f_z^{(1)} &= -\rho_1\, g + \delta_+(x,y,z)\,(\gamma_+)\,\kappa_+(x,y) + \delta_-(x,y,z)\left[(\gamma_-)\,\kappa_-(x,y) + \rho_2\, g\,\left(H^b - H + \frac{h}{2}\right)\right] \\
f_x^{(0)} &= 0 \\
f_y^{(0)} &= 0,
\end{aligned} \tag{3.3}$$

where $\delta_\pm(x,y,z) = \delta(z - z_\pm(x,y))$ denote the Dirac distributions centered on an interface $z = z_\pm(x,y)$, used here to account for surface forces, namely the capillary force and the force arising from pressure in the bath. In addition, we have introduced the following notation for the curvature of the lower and upper interfaces. :

$$\kappa_\pm(x,y) = \nabla^2 z_\pm(x,y) = \nabla^2\left(H(x,y) \pm \frac{h(x,y)}{2}\right).$$

We will refer to this case $\mathrm{Je} \ll 1$, $1/\mathrm{Ca} \ll 1$ and $t \sim (z^*)^2/(L\,U)$ as the BNT case.

(*b*) Alternatively, we consider the case where both the Jeffreys Je and inverse capillary 1/Ca numbers are large; transverse forces should be considered of order $1/\epsilon$, and are considered part of $f_z^{(-1)}$ in our equations. Since slope of the sheet is order ϵ, the projection of normal forces onto the (x,y) plane are of order ϵ^0, and enter into $f_x^{(0)}$ and $f_y^{(0)}$:

$$\begin{aligned}
f_z^{(-1)} &= -\rho_1 g + \delta_+(x,y,z)\,(\gamma_+)\,\kappa_+(x,y) + \delta_-(x,y,z)\left[(\gamma_-)\,\kappa_-(x,y) + \rho_2 g\left(H^b - H + \frac{h}{2}\right)\right] \\
f_z^{(1)} &= 0 \\
f_x^{(0)} &= \left(H + \frac{h}{2}\right)_{,x}(\gamma_+)\,\kappa_+(x,y) - \left(H - \frac{h}{2}\right)_{,x}\left[(\gamma_-)\,\kappa_-(x,y) + \rho_2 g\left(H^b - H + \frac{h}{2}\right)\right] \\
f_y^{(0)} &= \left(H + \frac{h}{2}\right)_{,y}(\gamma_+)\,\kappa_+(x,y) - \left(H - \frac{h}{2}\right)_{,y}\left[(\gamma_-)\,\kappa_-(x,y) + \rho_2 g\left(H^b - H + \frac{h}{2}\right)\right]
\end{aligned} \tag{3.4}$$

As explained in section 2.5, these large forces are studied at long times and using the Trouton scaling. We will simply refer to this case $\mathrm{Je} \gg 1$, $1/\mathrm{Ca} \gg 1$ and $t \sim L/U$ as the Trouton case.

These external forces are replaced into equations (2.31), (2.32) and (2.33). We keep

notations compact using the number $m = 0$ for the Trouton case and $m = 1$ for the BNT case. We obtain the following set of equations. First, mass conservation remains

$$h_{,t}(x,y) + (1-m)\left(\frac{\partial(\overline{u}(x,y)\,h(x,y))}{\partial x} + \frac{\partial(\overline{v}(x,y)\,h(x,y))}{\partial y}\right) = 0. \tag{3.5}$$

The in-plane force balance is obtained from equation (2.32), using the forces given in equations (3.4) and (3.3) integrated over thickness:

$$\begin{aligned} N_{xx,x} + N_{xy,y} &= -(1-m)\left(H+\frac{h}{2}\right)_{,x}(\gamma_+)\,\kappa_+(x,y) \\ &\quad +(1-m)\left(H-\frac{h}{2}\right)_{,x}\left[(\gamma_-)\,\kappa_-(x,y) + \rho_2\,g\left(H^b - H + \frac{h}{2}\right)\right] \end{aligned} \tag{3.6a}$$

$$\begin{aligned} N_{xy,x} + N_{yy,y} &= -(1-m)\left(H+\frac{h}{2}\right)_{,y}(\gamma_+)\,\kappa_+(x,y) \\ &\quad +(1-m)\left(H-\frac{h}{2}\right)_{,y}\left[(\gamma_-)\,\kappa_-(x,y) + \rho_2\,g\left(H^b - H + \frac{h}{2}\right)\right] \end{aligned} \tag{3.6b}$$

Inserting the forces in equations (3.4) and (3.3) into equation (2.34), and carrying out evaluation of the slice-based operators, we find the membrane stress:

$$\begin{aligned} N_{xx}(x,y) &= 2\mu\,h\,[2(\overline{u}_{,x} + m\,H_{,xt}\,H_{,x}) + \overline{v}_{,y} + m\,H_{,yt}\,H_{,y}] \\ &\quad + (1-m)\,h\,\frac{\gamma_+}{2}\,\kappa_+(x,y) - (1-m)\,h\,\frac{\gamma_-}{2}\,\kappa_-(x,y) \\ &\quad - (1-m)\,h\,\frac{\rho_2 g}{2}\left(H^b - H + \frac{h}{2}\right) \\ N_{xy}(x,y) &= \mu\,h\,[\overline{u}_{,y} + m\,H_{,xt}\,H_{,y} + \overline{v}_{,x} + m\,H_{,yt}\,H_{,x}] \\ N_{yy}(x,y) &= 2\mu\,h\,[\overline{u}_{,x} + m\,H_{,xt}\,H_{,x} + 2(\overline{v}_{,y} + m\,H_{,yt}\,H_{,y})] \\ &\quad + (1-m)\,h\,\frac{\gamma_+}{2}\,\kappa_+(x,y) - (1-m)\,h\,\frac{\gamma_-}{2}\,\kappa_-(x,y) \\ &\quad - (1-m)\,h\,\frac{\rho_2 g}{2}\left(H^b - H + \frac{h}{2}\right) \end{aligned} \tag{3.7}$$

In the Trouton case, the out-of-plane force balance (2.33a) boils down to

$$-(\gamma_+)\,\kappa_+(x,y) - (\gamma_-)\,\kappa_-(x,y) - \rho_2\,g\left(H^b - H + \frac{h}{2}\right) + \rho_1\,g\,h = 0 \quad (m=0), \tag{3.8a}$$

which is a partial differential equation for h and H. In the BNT case, we note that $[K \cdot f_z^{(-1)}](x,y) = 0$: we substitute the remaining terms in the expressions (2.35) of the moment, namely $M_{\alpha\beta}(x,y) = -(\mu\,h^3/3)\,(H_{,\alpha\beta t} + H_{,\gamma\gamma t}\,\delta_{\alpha\beta})/2$, into the transverse balance (2.33b), which yields:

$$\begin{aligned} N_{xx}\,H_{,xx} + 2N_{xy}\,H_{,xy} + N_{yy}\,H_{,yy} &= \frac{\mu\,h^3}{3}\,(H_{,xxxxt} + 2H_{,xxyyt} + H_{,y^4t})\cdots \\ -(\gamma_+)\,\kappa_+(x,y) - (\gamma_-)\,\kappa_-(x,y) - \rho_2\,g\left(H^b - H + \frac{h}{2}\right) + \rho_1\,g\,h &\quad (m=1) \end{aligned} \tag{3.8b}$$

3.2. *Base state*

We consider a flat configuration, $H(x,y,t) = H_0(t)$ and $h(x,y,t) = h_0(t)$ which is spatially uniform, but may evolve with time. The remainder of this paper is concerned with a *local* analysis of stability of this flat configuration. By 'local analysis', we mean that the typical scale of the in-plane flow is assumed to be much larger than the wavelength of the possibly unstable modes. The analysis is carried out over an intermediate length scale, where the strain rate $\mathbf{D}$ can be considered uniform.

An in-plane flow can be present in this flat state, and can be driven by forcing at the boundaries. In the remainder of the paper, our main goal is to compute growth rate of unstable modes, depending on the properties of this flow. To start with, we consider an in-plane flow that does not depend on time. This assumption can easily be relaxed: our expressions for the growth rate C as a function of the steady flow parameters α and β yield without modification the *instantaneous* growth rate as a function of the *current* flow parameters in the case of a time-dependent flow. This idea is implemented in full details in Section 5, see equation (5.2) in particular.

Let us call α and β the principal values of the 2D strain rate, ordered with the convention

$$\alpha < \beta. \tag{3.9}$$

By convention, the x and y axes are aligned with the associated principal directions. This makes the strain rate tensor diagonal, $D_{xx} = \alpha$, $D_{xy} = 0$ and $D_{yy} = \beta$. With this choice of axes, the in-plane velocity is given by

$$\begin{aligned} \overline{u}_0(x,y) &= \alpha\, x \\ \overline{v}_0(x,y) &= \beta\, y. \end{aligned} \tag{3.10}$$

In the right-hand side, we have omitted constants of integration representing a steady rigid-body motion, which do not affect the stability. Note that indices in parentheses, such as (0) in equation (2.23*a*) refer to the order in the expansion with respect to the small aspect-ratio. By contrast, indices without parentheses refer to the expansion associated with the analysis of stability: in equation above, $\overline{u}_0$ refers to the base solution, and $\overline{u}_1$, introduced next, to the perturbation (marginally stable mode).

Conservation of mass (3.5) reads, for our planar solution:

$$h_{0,t}(t) + (1-m)\,(\alpha+\beta)\,h_0(t) = 0. \tag{3.11}$$

In Trouton case ($m = 0$), the second term in non-zero and the thickness $h_0(t)$ of the base flow must depend explicitly on time, except in the special case of a pure shear flow ($\alpha + \beta = 0$).

In the absence of interface curvature, the transverse equilibrium (3.8*a*) or (3.8*b*) imposes the following buoyancy condition:

$$H_0(t) = H^b - \left(\frac{\rho_1}{\rho_2} - \frac{1}{2}\right)\, h_0(t). \tag{3.12}$$

Being homogeneous by assumption, the base state satisfies the in-plane force balance (3.6) automatically. The membrane stress is given by the constitutive law (3.7)

which reads, after substitution of equation (3.12):

$$N^0_{xx}(t) = 2\mu\,(2\alpha+\beta)\,h_0(t) - (1-m)\frac{\rho_1\,g\,h_0^2(t)}{2} \tag{3.13a}$$

$$N^0_{xy}(t) = 0 \tag{3.13b}$$

$$N^0_{yy}(t) = 2\mu\,(\alpha+2\beta)\,h_0(t) - (1-m)\frac{\rho_1\,g\,h_0^2(t)}{2} \tag{3.13c}$$

This unperturbed membrane stress will appear in the equations for the linear stability.

3.3. *Perturbation*

We seek solutions to the equations (3.5–3.8) by perturbing this spatially homogeneous base state:

$$h(x,y,t) = h_0(t) \;+ h_1(x,y,t) \tag{3.14a}$$

$$H(x,y,t) = H_0(t) + H_1(x,y,t) \tag{3.14b}$$

$$\overline{u}(x,y,t) = \alpha\,x \quad + \overline{u}_1(x,y,t) \tag{3.14c}$$

$$\overline{v}(x,y,t) = \beta\,y \quad + \overline{v}_1(x,y,t) \tag{3.14d}$$

where $h_0(t)$, $H_0(t)$, $\overline{u}_0 = \alpha\,x$ and $\overline{v}_0 = \beta\,y$ characterize the flat base state of the previous section, and $h_1(x,y,t)$, $H_1(x,y,t)$, $\overline{u}_1(x,y,t)$, $\overline{v}_1(x,y,t)$ stand for the perturbations to thickness, mid-surface, and velocity.

As an illustration, we consider the case where the in-plane velocity is imposed at the boundaries, which is far from the region of interest. In view of this, the perturbation to velocity should vanish at infinity:

$$\begin{aligned} \lim_{(x,y)\to\infty} \overline{u}_1(x,y) &= 0 \\ \lim_{(x,y)\to\infty} \overline{v}_1(x,y) &= 0. \end{aligned} \tag{3.15}$$

The stability is investigated next. In Section 4 we treat the BNT case and find that the most unstable modes are purely undulatory (thickness h remains constant); in Section 5 we study the Trouton case, and find that the unstable modes couple thickness and height variations.

4. Small forces, short time: undulatory perturbation

In this Section we study the linear stability of the flat configuration under the scaling assumptions (a) of Section 3.1, namely the BNT case ($m = 1$) with small transverse forces and short time.

4.1. *Linear stability analysis*

By equation (3.5), the thickness remains unperturbed when $m = 1$:

$$h_1(x,y,t) = 0. \tag{4.1}$$

Physically, this means that perturbations to thickness become significant on time scales that are much larger than those considered in the BNT case.

In the constitutive equation for membrane stress (3.7) all the non-linear terms relevant to BNT case, such as $H_{,x}\,H_{,xt}$, appear as second-order quantities. Reading off the

equation to first order, we have

$$\begin{aligned} N^1_{xx}(x,y) &= 2\mu\, h_0\ [2\overline{u}_{1,x}(x,y) + \overline{v}_{1,y}(x,y)] \\ N^1_{xy}(x,y) &= \mu\, h_0\ [\overline{u}_{1,y}(x,y) + \overline{v}_{1,x}(x,y)] \\ N^1_{yy}(x,y) &= 2\mu\, h_0\ [\overline{u}_{1,x}(x,y) + 2\overline{v}_{1,y}(x,y)]\,. \end{aligned} \tag{4.2}$$

These quantities are subjected to the in-plane equilibrium conditions (3.6) which for $m = 1$ are homogeneous equations:

$$\begin{aligned} N^1_{xx,x}(x,y) + N^1_{xy,y}(x,y) &= 0 \\ N^1_{xy,x}(x,y) + N^1_{yy,y}(x,y) &= 0. \end{aligned} \tag{4.3}$$

Together with the asymptotic conditions (3.15), these two equations (4.2) and (4.3) constitute a well-posed problem for the velocities $\overline{u}_1$ and $\overline{v}_1$, which is uncoupled from the transverse quantities h_1 and H_1 (this decoupling is classical in the analysis of buckling near flat configurations, and comes from the up-down symmetry). Note that the time derivatives $\overline{u}_{1,t}$ or $\overline{v}_{1,t}$ do not show up in the above set of equations. In fact, we recognize the equations of 2D, linearized elasticity when $\overline{u}_1$ and $\overline{v}_1$ are identified with displacement, and μ with an elastic modulus. With this analogy, equations (3.15) impose clamping conditions at infinity; then, we know that the only solution is the trivial one:

$$\overline{u}_1(x,y) = 0, \qquad \overline{v}_1(x,y) = 0, \tag{4.4}$$

for all values of x and y. Under the present assumptions, unstable modes are purely transverse.

Upon linearization, the transverse force balance (3.8*b*) provides an equation for the deflection H_1 which is decoupled from in-plane flow:

$$\begin{aligned} h_0\,[2(2\alpha+\beta)\,H_{1,xx} + 2(\alpha+2\beta)\,H_{1,yy}] = \frac{1}{3}\,h_0^3\,(H_{1,xxxxt} + 2H_{1,xxyyt} + H_{1,y^4t})\cdots \\ - \frac{\gamma_+ + \gamma_-}{\mu}(H_{1,xx} + H_{1,yy}) + \frac{\rho_2\, g}{\mu}\,H_1. \end{aligned} \tag{4.5}$$

Here, we have replaced in the expressions (3.13) for the unperturbed membrane stress, and have linearized the non-linear terms using equalities such as $(N_{xx}\,H_{,xx})_1 = N^0_{xx}\,H_{1,xx}$ since $H_{0,xx} = 0$.

The coefficients in linear equation (4.5) are independent both of time and space, and we seek a solution of the form

$$H_1(x,y,t) = \hat{H}_1\, e^{C_{\rm u}\,t + i\,\mathbf{k}\cdot\mathbf{x}}, \tag{4.6}$$

where $\hat{H}_1$ is a complex amplitude, $C_{\rm u}$ is the growth rate to be determined later, $\mathbf{k} = (k_x, k_y)$ is the spatial wavenumber, and $\mathbf{x} = (x,y)$ the in-plane coordinate. We seek the wavevector in cylindrical coordinates,

$$k_x = k\,\cos\theta, \qquad k_y = k\,\sin\theta, \tag{4.7}$$

where $\theta = 0$ corresponds to $\mathbf{k}$ aligned with the x axis, *i. e.* with the smallest eigenvalue α of the shear rate tensor $\mathbf{D}$.

Substituting the trial form (4.6) into equation (4.5), we find an expression for the growth rate

$$C_{\rm u}(k,\theta) = \frac{6}{(h_0\,k)^2}\left[-\alpha\,(1+\cos^2\theta) - \beta\,(1+\sin^2\theta) - \frac{1}{(h_0\,k)^2}\left(\frac{(\gamma_+ + \gamma_-)\,h_0\,k^2 + \rho_2\,g\,h_0}{2\mu}\right)\right] \tag{4.8}$$

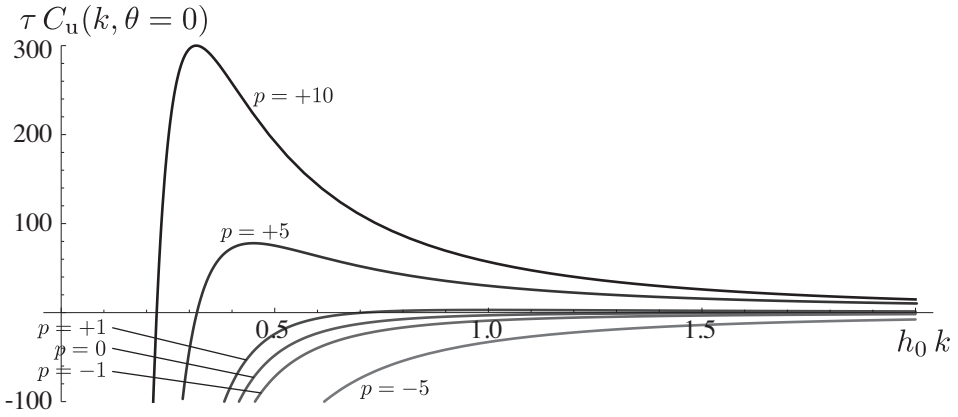

FIGURE 4. Dimensionless growth rate ($\tau\, C_{\rm u}$) for the undulatory perturbation, plotted from equation (4.9) as a function of the dimensionless wavenumber ($h_0\, k$). The most unstable direction $\theta = 0$ is considered.

A positive growth rate corresponds to an instability. For a given base flow, the wavevector corresponding to the most unstable mode is found by maximizing $C_{\rm u}(k, \theta)$ with respect to k and θ. By a convention expressed by equation (3.9), we have $\alpha < \beta$; as a result, the maximum of $C_{\rm u}$ with respect to θ is always reached for $\theta = 0$. Then, the wavenumber $\mathbf{k}$ is aligned with the x axis, and the instability pattern is made of stripes perpendicular to the x axis, see the inset in figure 5. This orientation of the pattern is characteristic of a buckling phenomenon as the x axis is the direction of most vigorous contraction — in the sense that $-\alpha > -\beta$ by equation (3.9).

Setting $\theta = 0$ in the equation above yields

$$\tau\, C_{\rm u}(k, \theta = 0) = \frac{6}{(h_0\, k)^2} \left[p - \frac{1}{2\,(h_0\, k)^2} \right], \tag{4.9}$$

where we have introduced the characteristic times obtained by balancing viscous effects and gravity, τ, and viscous effects and surface tension, τ_2, the Bond number, $\mathcal{C}$, and the control parameter, p; those parameters are defined by

$$\tau = \frac{\mu}{\rho_2\, g\, h_0}, \qquad \tau_2 = \frac{h_0\, \mu}{\gamma_+ + \gamma_-}, \qquad \mathcal{C} = \frac{\tau_2}{\tau}, \qquad p = -\tau\,(2\,\alpha + \beta) - \frac{1}{2\,\mathcal{C}}. \tag{4.10}$$

They are all fixed once the base state is prescribed.

Typical plots of the growth rate $C_{\rm u}(k, 0)$ given by equation (4.9) as a function of wavelength k are shown in figure 4. For $p < 0$, $C_{\rm u}$ is negative for any value of k and the planar base state is linearly stable. For $p > 0$ however, there is a range of unstable wavelengths; the maximal value of the growth rate $C_{\rm u}^{\rm max}$ and the associated wavelength $k_{\rm max}$ satisfy the following relations:

$$\tau\, C_{\rm u}^{\rm max} = 3\, p^2, \qquad h_0\, k_{\rm max} = \frac{1}{p^{\frac{1}{2}}} \qquad (p > 0), \tag{4.11}$$

that is, in physical units:

$$C_{\mathrm{u}}^{\max} = \frac{3\,\mu}{\rho_2\,g\,h_0}\left[-(2\,\alpha+\beta) - \frac{\gamma_+ + \gamma_-}{2\,h_0\,\mu}\right]^2, \qquad k_{\max} = \frac{\left(\frac{\rho_2\,g}{h_0\,\mu}\right)^{\frac{1}{2}}}{\left[-(2\,\alpha+\beta) - \frac{\gamma_+ + \gamma_-}{2\,h_0\,\mu}\right]^{\frac{1}{2}}}. \tag{4.12}$$

These expressions apply to the case $p > 0$, that is when the argument of the square bracket is positive.

A stability diagram is plotted in figure 5 as a function of the flow properties. The curve corresponding to the loss of stability is given by the equation $p = 0$ for $\alpha < \beta$, and is thus a straight line in the upper-left part of the diagram. We complement the other half of the diagram, $\alpha > \beta$, by symmetry: in this region, the parameters α and β have to be swapped in the previous analysis to comply with equation (3.9). The angular point in the boundary correspond to a change of orientation of the most unstable vector $\mathbf{k}$ by an angle $\pi/2$ when the principal values of the strain rate α and β cross each other. Note that the planar state is always stable when hen the flow is extensional along both its principal directions ($\alpha > 0$ and $\beta > 0$, implying $p < 0$). In the unstable regions, a buckling instability is driven by compressive membrane stress (when the flow is such that $\alpha < 0$ and/or $\beta < 0$), and resisted by buoyancy and surface tension: from equation (4.8), buoyancy is stabilizing at large values of the wavelength $2\pi/k$, while surface tension stabilizes relatively smaller wavelengths. As a result, the instability threshold depends on surface tension and buoyancy.

The thin sheet approximation used here assumes that the wavelength is large compared to the thickness, $h_0\,k \ll 1$. By equation (4.11), this requires that the parameter p is significantly larger than unity too. A limit case is when gravity vanishes, or when the compressive strain is high; the wavelength becomes large, and can even become comparable to the the lateral size of the system; the growth rate becomes large as well. This case corresponds to the observations of Taylor (1968) on compressed viscous threads, where the observed wavelength is comparable to the size of the object undergoing compression.

We also recover the results of the linear stability of Benjamin & Mullin (1988), who used the equations for volumetric viscous fluids (3D) to interpret Taylor's experiment on the wrinkling of a sheared, floating annulus (Taylor 1968). The thin sheet model used here makes the analysis considerably simpler, as there is no need to solve for the transverse dependence of the various quantities. We checked that the matrix in equation (28) obtained by Benjamin & Mullin (1988) assuming pure shear, yields our dispersion relation when expanded in the thin sheet limit ($h_0\,k \ll 1$) in the special case $\beta = -\alpha$ (pure shear).

In addition to providing a set of equations that can be readily applied to a variety of geometries, our framework can be used to address the non-linear dynamics of thin sheets, as shown in the following section.

4.2. *Non-linear stability analysis*

The linear stability analysis of the previous section predicts an exponential increase of the amplitude when the flow is unstable. For large amplitudes, linearization breaks down and a non-linear analysis is required. The wavevector of the most unstable mode is along the x axis, which is by our orientation of axes the direction achieving the most vigorous contraction, see equation (3.9). We perform a non-linear study of the most unstable mode, assuming that the invariance of the linear mode along the y direction carries on

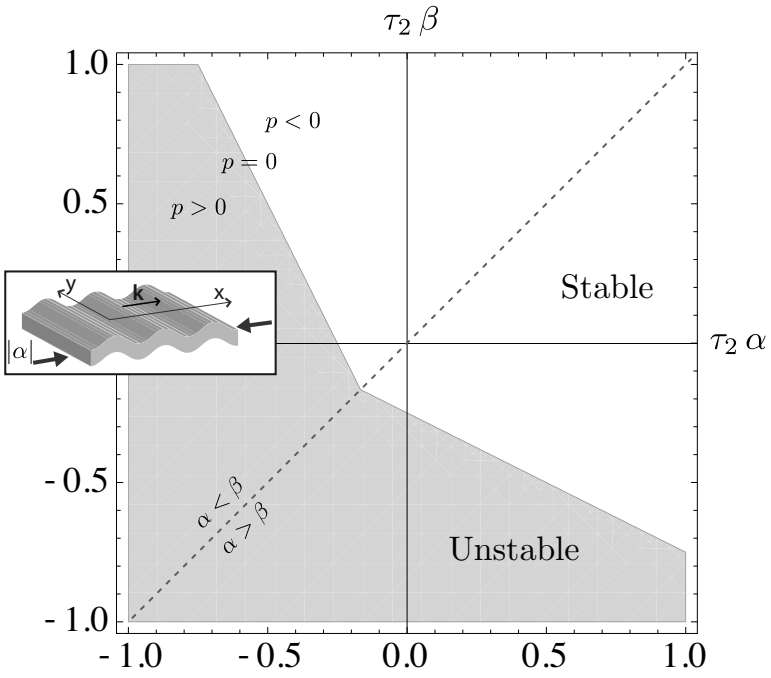

FIGURE 5. Stability with respect to buckling as a function of the principal values of strain rate (α, β), rescaled using the parameter $\tau_2 = \tau\,\mathcal{C}$. The buckling condition $p > 0$ defined in equation (4.11) has been rewritten $2\,(\tau_2\,\alpha) + (\tau_2\,\beta) > -1/2$ using equation (4.10). This equation holds with the convention of axes defined in the main text, for which $\alpha < \beta$. The diagram has been extended below the dashed diagonal by mirror symmetry.

to the non-linear regime:

$$H_{,y}(x,y,t) = 0, \quad N_{ij,y}(x,y,t) = 0, \quad \overline{u}_{,y}(x,y,t) = 0, \quad \overline{v}_{,y}(x,y,t) = 0, \tag{4.13}$$

where the in-plane indices i and j for N_{ij} can take on the values x or y. We seek the solutions H in the form (for the method, see e.g. Manneville 2004; Charru 2007)

$$H(x,t) = H_0(t) + \frac{1}{2}\,\left(A(t)\,e^{ik_{\max}\,x} + A^*(t)\,e^{-ik_{\max}\,x}\right), \tag{4.14}$$

where $A(t)$ is the complex amplitude of the pattern.

Before starting the calculation, we need to modify the asymptotic condition (3.15) for the in-plane velocity. Requiring convergence of velocity (u, v) to the reference flow $(\alpha\,x, \beta\,y)$ is appropriate at linear order, but not at second order. If imposed at second order, it has the unwanted effect to suppress the instability: by equation (4.21), growth of the cylindrical pattern is accompanied by a second-order in-plane velocity which is small and oscillatory, and does not converge to zero asymptotically for $(x, y) \to \infty$. To work around this, we require the following condition to hold at any time t:

$$\langle \overline{u}_{,x} \rangle_x(y) = \alpha \quad \text{for all } y, \qquad \langle \overline{v}_{,y} \rangle_y(x) = \beta \quad \text{for all } x. \tag{4.15}$$

Here, $\langle f\rangle_x(y_0)$ denotes the average of a function $f(x,y)$ over the line with equation $y=y_0$, and its average $\langle f\rangle_x(x_0)$ over the line with equation $x=x_0$. Since equation (4.15) involves the averages of derivatives over an infinite domain, it is equivalent to the mild assumption that the difference between $\overline{u}(x,y)$ and $\alpha\,x$, and between $\overline{v}(x,y)$ and $\beta\,y$, remains bounded. The aim of equation (4.15) is to prevent any systematic deviation from the reference solution $\overline{u}=\alpha\,x$ and $\overline{v}=\beta\,y$, and in this sense is in line with the former asymptotic condition (3.15).

Let us observe that the constitutive relations (3.7) for N_{xx} and N_{yy} can be solved for $u_{,x}$ and $v_{,y}$: with $m=1$ and $H_{,y}=0$, this yields

$$\overline{u}_{,x}(x,y,t)=\frac{2\,N_{xx}(x,y,t)-N_{yy}(x,y,t)}{6\,\mu\,h}-H_{,xt}(x,y,t)\,H_{,x}(x,y,t) \tag{4.16a}$$

$$\overline{v}_{,y}(x,y,t)=\frac{-N_{xx}(x,y,t)+2\,N_{yy}(x,y,t)}{6\,\mu\,h} \tag{4.16b}$$

By the invariance condition (4.13), all terms in the right-hand side of equation (4.16*b*) are actually independent of y, and so is $\overline{v}_{,y}$ too, $\overline{v}_{,y}(x,y)=\overline{v}_{,y}(x)$. This implies that averaging over y has no effect on $\overline{v}_{,y}$: $\langle\overline{v}_{,y}\rangle_y(x)=\overline{v}_{,y}(x)$. Combining with equation (4.15), we have

$$\overline{v}_{,y}(x,y,t)=\beta, \tag{4.17}$$

for any x, y and t: this component of the in-plane velocity remains unperturbed at all orders.

Substituting this expression into the constitutive equation (3.7) for N_{xx}, we have ($m=1$):

$$N_{xx}(x,y,t)=2\,\mu\,h\,\left(2\,\overline{u}_{,x}+\beta+2\,H_{,xt}\,H_{,x}\right). \tag{4.18}$$

By the invariance (4.13), all terms in this equation are actually independent of y. Averaging over x, we obtain

$$\langle N_{xx}\rangle_x(t)=2\,\mu\,h\,\left(2\,\alpha+\beta+2\,\langle H_{,xt}\,H_{,x}\rangle_x(t)\right), \tag{4.19a}$$

after simplification of $\langle\overline{u}_{,x}\rangle_x$ using equation (4.15). Calculation of the average in the right-hand side is straightforward from equation (4.14):

$$\langle H_{,xt}\,H_{,x}\rangle_x(t)=+\frac{k_{\max}^2}{2}\,|A(t)|\,\frac{\mathrm{d}|A(t)|}{\mathrm{d}t}. \tag{4.19b}$$

Using the invariance (4.13), the in-plane equilibrium condition (3.6*a*) boils down for $m=1$ to $N_{xx,x}(x,y,t)=0$: N_{xx} is independent of x, and we have

$$N_{xx}(x,y,t)=\langle N_{xx}\rangle_x(y,t) \tag{4.19c}$$

Combining the three above equations (4.19*a*–4.19*c*), we find the value of the stress N_{xx}:

$$N_{xx}(x,y,t)=2\,\mu\,h\,\left((2\,\alpha+\beta)+k_{\max}^2\,|A(t)|\,\frac{\mathrm{d}|A(t)|}{\mathrm{d}t}\right), \tag{4.20}$$

a quantity which appears to be uniform in space. The last term in the parenthesis provides a non-linear correction to the unperturbed membrane stress N_{xx}^0 given in equation (3.13*a*).

The in-plane velocity $\overline{u}$ can be reconstructed from equation (4.18) by combining equations (4.14) and (4.20):

$$\overline{u}_{,x}=\alpha+\frac{k_{\max}^2}{2}\,\left(\frac{A\,\dot{A}^*\,e^{2\,i\,k_{\max}\,x}+\dot{A}\,A^*\,e^{-2\,i\,k_{\max}\,x}}{2}\right). \tag{4.21}$$

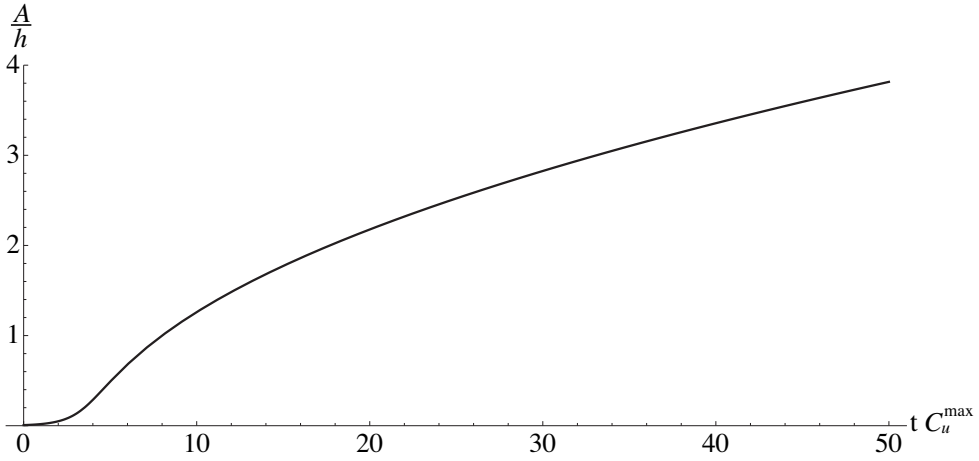

FIGURE 6. Time evolution of the amplitude of the undulatory mode predicted by the non-linear analysis (4.24): dimensionless amplitude as a function of dimensionless time.

As announced this expression contains a constant part equal to the imposed average value, α, plus a second-order oscillatory part.

After dropping all terms involving some derivative along y, the transverse force balance (4.5) reads

$$\frac{\mu\, h^3}{3}\, H_{,xxxxt} - (\gamma_+ + \gamma_-)\, H_{,xx} + \rho_2\, g\, H = N_{xx}\, H_{,xx}. \tag{4.22}$$

We now substitute into this equation the expressions (4.14) for H and (4.20) for N_{xx}. This yields a differential equation for the evolution of the amplitude,

$$\frac{\mu\, h^3}{3}\, k_{\max}^4\, \frac{1}{A}\frac{\mathrm{d}|A(t)|}{\mathrm{d}t} + (\gamma_+ + \gamma_-)\, k_{\max}^2 + \rho_2\, g = 2\,\mu\, h\, \left((2\,\alpha + \beta) + k_{\max}^2\, |A(t)|\, \frac{\mathrm{d}|A(t)|}{\mathrm{d}t} \right)\, (-k_{\max}^2).$$

Using the dimensionless parameters introduced in equation (4.10), this differential equation can be rewritten as:

$$\frac{(h\, k_{\max})^4}{6}\, \tau\, \frac{1}{A}\frac{\mathrm{d}|A(t)|}{\mathrm{d}t} = (h\, k_{\max})^2\, p - \frac{1}{2} - \frac{\tau\, (h\, k_{\max})^4}{h^2}\, |A(t)|\, \frac{\mathrm{d}|A(t)|}{\mathrm{d}t}$$

This expression can be simplified using the definitions of $C_{\mathrm{u}}^{\max}$ and $k_{\max}$ in equation (4.11):

$$\frac{\mathrm{d}|A(t)|}{\mathrm{d}t} = C_{\mathrm{u}}^{\max}\, A(t) - \frac{6}{h^2}\, |A(t)|\, \frac{\mathrm{d}|A(t)|}{\mathrm{d}t}\, A(t). \tag{4.23}$$

The exponential growth rate predicted by linear theory, $A_{,t} = C_{\mathrm{u}}^{\max}\, A$, is recovered when the non-linear term is omitted.

The complex argument of any solution $A(t)$ of equation (4.23) being conserved during time, $A(t)$ can be assumed to be real positive without loss of generality. The general solution of this equation is given by the following implicit equation:

$$\ln \frac{A(t)}{h} + 3\, \frac{A^2(t)}{h^2} = C_{\mathrm{u}}^{\max}\, (t - t_0) \tag{4.24}$$

where t_0 is a constant of integration. This solution $A(t)$ is plotted in Figure 6.

Equation (4.24) describes the transition from exponential growth $A(t) = A_0 \exp(C_{\mathrm{u}}^{\max}\, t)$ at short times, to square root growth $A(t) = h\, (C_{\mathrm{u}}^{\max}\, t/3)^{1/2}$ at long times. The transition

occurs when the amplitude reaches a value comparable to the thickness, $A/h \approx 1$, corresponding to $t - t_0 \sim 1/C_{\mathrm{u}}^{\max}$. Note that the wavelength of the pattern, $2\pi/k_{\max} \sim h\,p^{1/2}$, is much larger than the deflection h at the cross-over between the two regimes: using the small slope approximation is consistent in the limit $|p| \gg 1$ which we consider here; it remains valid until time t becomes comparable to the large time $\frac{p}{C_{\mathrm{u}}^{\max}}$, which is when the amplitude of the pattern would become comparable to wavelength.

The square-root growth of the amplitude can be explained by the kinematics of inextensional wrinkling: the parenthesis in the right-hand side of equation (4.20) is the strain rate D_{xx}. For inextensional wrinkling, settings $D_{xx} = 0$ yields the scaling $A \sim t^{\frac{1}{2}}$. This square-root behavior is also compatible with the non-linear analysis of a thin viscous thread by Buckmaster *et al.* (1975).

We considered the pattern whose wavelength is fixed by the criterion of maximal growth rate in the framework of a linear stability analysis. A non-linear analysis revealed that the exponential growth at short times predicted by linear theory is limited by non-linear effects: when the deflection becomes comparable to thickness of the sheet, the amplitude grows more slowly, like the square-root of time.

5. Large forces, long time: coupled perturbation

We study the stability of the planar solution given in Section 3.2, and consider the Trouton case, that is large transverse forces and long time. We carry out as earlier a local stability analysis, and consider the in-plane velocity field $(\overline{u}_0, \overline{v}_0)$ given by equation (3.10), which depends linearly on the coordinates x and y. In Trouton model, we can no longer ignore the evolution of thickness with time due to the 2D divergence of the base flow: the solution of equation (3.11) is

$$h_0(t) = h_0(0)\, e^{-(\alpha+\beta)\, t}. \tag{5.1}$$

Because of the explicit time dependence of the base solution (5.1), the simple exponential dependence assumed earlier in equation (4.6) is no longer applicable. We consider the more general form:

$$H_1(x,y,t) = \hat{H}_1\, e^{\Sigma(t) + i\,\mathbf{k}(t)\cdot\mathbf{x}} \tag{5.2a}$$

$$h_1(x,y,t) = \hat{h}_1\, e^{\Sigma(t) + i\,\mathbf{k}(t)\cdot\mathbf{x}} \tag{5.2b}$$

$$\overline{u}_1(x,y,t) = i\,\hat{u}_1\, e^{\Sigma(t) + i\,\mathbf{k}(t)\cdot\mathbf{x}} \tag{5.2c}$$

$$\overline{v}_1(x,y,t) = i\,\hat{v}_1\, e^{\Sigma(t) + i\,\mathbf{k}(t)\cdot\mathbf{x}} \tag{5.2d}$$

for the perturbed quantities H_1, h_1, $\overline{u}_1$ and $\overline{v}_1$ introduced in equation (3.14). The first term in the exponential is the integrated growth rate:

$$\Sigma(t) = \int_0^t C_{\mathrm{c}}(\tilde{t})\,\mathrm{d}\tilde{t}. \tag{5.2e}$$

We anticipate that the equation governing $C_{\mathrm{c}}(t)$ is simpler than that for $\Sigma(t)$, and shall eliminate Σ in favor of C_{c} whenever possible. Note that we have also kept an explicit dependence of the wavevector $\mathbf{k}(t)$ on time, for a reason that will soon be clear.

We can factor out the complex exponentials in equation (5.2) and introduce the fol-

lowing representation of the derivative operators:

$$\partial_t = C_{\rm c}(t) + i\,\mathbf{k}'(t)\cdot\mathbf{x} \tag{5.3a}$$
$$\partial_x = i\,k_x(t) \tag{5.3b}$$
$$\partial_y = i\,k_y(t). \tag{5.3c}$$

Mass conservation (3.5) yields, at first order

$$(C_{\rm c}+i\,\mathbf{k}'(t)\cdot\mathbf{x})\,\hat{h}_1+(\alpha+\beta)\,\hat{h}_1-h_0\,(k_x(t)\,\hat{u}_1+k_y(t)\,\hat{v}_1)+i\,(\overline{u}_0(x)\,k_x(t)+\overline{v}_0(y)\,k_y(t))\,\hat{h}_1=0. \tag{5.4}$$

Here we would have expected an algebraic equation for the amplitudes $\hat{h}_1$, $\hat{u}_1$ and $\hat{v}_1$, but find an additional dependence on the coordinates $\mathbf{x}=(x,y)$ through the terms $\mathbf{k}'(t)\cdot\mathbf{x}$, $\overline{u}_0(x)=\alpha\,x$ and $\overline{v}_0(y)=\beta\,y$. For this equation to be satisfied for any value of (x,y), we first require that the coefficients of x and y vanish. This yields $k_x'(t)+\alpha\,k_x=0$ and $k_y'(t)+\beta\,k_y=0$ which writes, in intrinsic variables,

$$\frac{\partial\mathbf{k}(t)}{\partial t} = -\mathbf{D}(t)\cdot\mathbf{k}(t). \tag{5.5}$$

Equation (5.5) specifies the dilation and rotation of the wavenumber $\mathbf{k}(t)$ by the flow, and generalizes the 1D derivation of Smith (1975). A similar equation has been used in combustion theory: in their equation (40), Zel'dovich *et al.* (1980) capture the effect of a velocity gradient on the growth rate of a harmonic perturbation advected along an expanding flame surface, which they call the stretch-effect. We note that equation (5.5) can be interpreted as the conservation of the phase of the unstable mode by the co-moving derivative:

$$\left(\frac{\partial}{\partial t}+\overline{u}_0\,\frac{\partial}{\partial x}+\overline{v}_0\,\frac{\partial}{\partial y}\right)(\mathbf{k}(t)\cdot\mathbf{x})=0.$$

In this form, the equation appears to be related to the condition of advection of the phase of a WKB expansion in the analysis of short scale perturbations in fluid mechanics, see for instance equation (7) of Lifschitz & Hameiri (1991).

When the advection condition (5.5) for the wavenumber is taken into account, the mass conservation (5.4) simplifies to:

$$[C_{\rm c}+\alpha+\beta]\,\hat{h}_1+[-h_0(t)\,k_x(t)]\,\hat{u}_1+[-h_0(t)\,k_y(t)]\,\hat{v}_1=0 \tag{5.6}$$

By the linearized balance of transverse force (3.8a), we have:

$$\left[\rho_1\,g-\frac{\rho_2\,g}{2}+k^2(t)\,\frac{\gamma_+-\gamma_-}{2}\right]\,\hat{h}_1+\left[k^2(t)\,(\gamma_++\gamma_-)+\rho_2\,g\right]\,\hat{H}_1=0 \tag{5.7}$$

At linear order, the in-plane force balance (3.6) yields:

$$i\,k_x\,\hat{N}^1_{xx}+i\,k_y\,\hat{N}^1_{xy}=\rho_1\,g\,h_0(t)\,(i\,k_x(t))\,\left(\hat{H}_1-\frac{\hat{h}_1}{2}\right) \tag{5.8a}$$
$$i\,k_x\,\hat{N}^1_{xy}+i\,k_y\,\hat{N}^1_{yy}=\rho_1\,g\,h_0(t)\,(i\,k_y(t))\,\left(\hat{H}_1-\frac{\hat{h}_1}{2}\right), \tag{5.8b}$$

after simplifying the right-hand sides using the buoyancy condition (3.12). The linearized

membrane stress $\hat{N}^1_{ij}$ is given by the constitutive relations (3.7)

$$\hat{N}^1_{xx} = h_0 \left(-2\mu \left(2\,\hat{u}_1\,k_x + \hat{v}_1\,k_y \right) - \frac{(\gamma_+ - \gamma_-)}{2}\,k^2\,\hat{H}_1 - \frac{(\gamma_+ + \gamma_-)}{4}\,k^2\,\hat{h}_1 - \frac{\rho_2 g}{2}\left(-\hat{H}_1 + \frac{\hat{h}_1}{2} \right) \right)$$
$$\cdots + \left(2\mu\,(2\alpha + \beta) - \frac{\rho_1\,g\,h_0}{2} \right)\,\hat{h}_1 \qquad (5.9a)$$
$$\hat{N}^1_{xy} = -\mu\,h_0\,(\hat{u}_1\,k_y + \hat{v}_1\,k_x) \qquad (5.9b)$$
$$\hat{N}^1_{yy} = h_0 \left(-2\mu \left(\hat{u}_1\,k_x + 2\,\hat{v}_1\,k_y \right) - \frac{(\gamma_+ - \gamma_-)}{2}\,k^2\,\hat{H}_1 - \frac{(\gamma_+ + \gamma_-)}{4}\,k^2\,\hat{h}_1 - \frac{\rho_2 g}{2}\left(-\hat{H}_1 + \frac{\hat{h}_1}{2} \right) \right)$$
$$\cdots + \left(2\mu\,(\alpha + 2\beta) - \frac{\rho_1\,g\,h_0}{2} \right)\,\hat{h}_1 \qquad (5.9c)$$

With the aim to formulate the stability problem in dimensionless form, we recall the characteristic times τ and τ_2 from equation (4.10), and introduce two new parameters τ_3 and τ_4:

$$\tau = \frac{\mu}{\rho_2\,g\,h} \quad \tau_2 = \frac{h\,\mu}{\gamma_+ + \gamma_-} \quad \tau_3 = \frac{\mu}{(2\rho_1 - \rho_2)\,g\,h} \quad \tau_4 = \frac{h\,\mu}{\gamma_+ - \gamma_-}. \qquad (5.10)$$

In complement to $\mathcal{C} = \tau_2/\tau$ and p, we introduce another Bond number $\mathcal{C}_2 = \tau_4/\tau_3$, and the control parameter R:

$$\mathcal{C} = \frac{h^2\,\rho_2\,g}{\gamma_+ + \gamma_-} \quad \mathcal{C}_2 = \frac{h^2\,(2\rho_1 - \rho_2)\,g}{\gamma_+ - \gamma_-} \quad R(\theta) = -\frac{\alpha \sin^2\theta + \beta \cos^2\theta}{2}. \qquad (5.11)$$

The set of equations (5.6–5.9) write, after elimination of the membrane stress $\hat{N}_{ij}$:

$$\mathbf{M} \cdot \begin{pmatrix} \hat{h}_1 \\ \hat{H}_1 \\ \hat{u}_1 \\ \hat{v}_1 \end{pmatrix} = \begin{pmatrix} 0 \\ 0 \\ 0 \\ 0 \end{pmatrix}, \qquad (5.12)$$

$\mathbf{M}$ being defined by

$$\mathbf{M} = \begin{pmatrix} C_{\mathrm{c}} + \alpha + \beta & 0 & -c\,k\,h_0 & -s\,k\,h_0 \\ A_1 & 2A_2 & 0 & 0 \\ \left(2(2\alpha+\beta) - \frac{1}{4}A_2\right)c & -\frac{c}{2}A_1 & -h_0 k(3c^2+1) & -3h_0 ksc \\ \left(2(\alpha+2\beta) - \frac{1}{4}A_2\right)s & -\frac{s}{2}A_1 & -3h_0 ksc & -h_0 k(3s^2+1) \end{pmatrix}, \qquad (5.13)$$

where $A_1 = \dfrac{1}{\tau_3} + \dfrac{h_0^2 k^2}{\tau_4}$, $A_2 = \dfrac{1}{\tau} + \dfrac{h_0^2 k^2}{\tau_2}$, $s = \sin\theta$ and $c = \cos\theta$, the angle θ between the x axis and the wavevector $\mathbf{k}(t)$ being defined in equation (4.7).

The existence of a solution to the linearized equations (5.12) requires the determinant

of $\mathbf{M}$ to vanish. This condition yields an equation for the growth rate $C_{\rm c}(k,\theta)$

$$\tau\, C_{\rm c}(k,\theta) = \tau\, R(\theta) + \frac{1}{16}\left[\left(\frac{\tau}{\tau_3}\right)^2 \frac{\left(1+\dfrac{(h\,k)^2}{\mathcal{C}_2}\right)^2}{1+\dfrac{(h\,k)^2}{\mathcal{C}}} - \left(1+\frac{(h\,k)^2}{\mathcal{C}}\right)\right]. \tag{5.14}$$

The case of pure shear flow ($\alpha = -\beta$) has been studied by Benjamin & Mullin (1988); for this type of flow, the above value of the growth factor $C_{\rm c}$ can be recovered from matrix defined in their equation (28) in the thin sheet limit ($h\,k \ll 1$). The set of equations presented here are valid for an arbitrary base flow.

The growth factor $C_{\rm c}$ is of variable sign depending on the value of the parameters. The first term in the right-hand side, proportional to $R(\theta)$, describes the effect of the in-plane flow, and is destabilizing for contractile flows. The first term in the square bracket is destabilizing and originates in the coupling between the two faces of the sheet. The second term (-1) in the square bracket describes the stabilization of all wavelengths by gravity, while the last term in the square bracket, proportional to $(hk)^2/\mathcal{C}$, accounts for the stabilization by surface tension, which is effective for short wavelengths.

With our convention $\alpha < \beta$, the growth factor $C_{\rm c}$ is maximum when the wavevector $\mathbf{k}$ is aligned with the y axis, that is $\theta = \frac{\pi}{2}$. Indeed, this makes the only term depending on θ, namely $\tau\, R(\theta)$, maximum by equation (5.11). In the absence of external forces, *i. e.* for a free-standing sheet, the square bracket cancels and the planar flow becomes unstable as soon as there exists a contractile direction in the base flow ($\alpha < 0$, $R(\pi/2) > 0$).

In figures 7 and 8, we have restored the external forces, but consider the particular case $\gamma_+ = \gamma_-$ and $\rho_2 = \rho_1$, for which:

$$\frac{\tau}{\tau_3} = 1, \qquad \frac{1}{\mathcal{C}_2} = 0. \tag{5.15}$$

In that case, equation (5.14) yields $\tau\, C_{\rm c}(k,\theta) = \tau\, R(\theta) + (\breve{k}^{-1} - \breve{k})/16$ with $\breve{k} = 1 + (h\,k)^2/\mathcal{C} \geq 1$. The maximum with respect to the wavenumber is reached $\breve{k} = 1$, that is $k = 0$; the maximum with respect to the direction is reached for $\theta = \frac{\pi}{2}$. The stability is therefore determined by the sign of

$$\tau\, C_{\rm c}\left(k = 0, \theta = \frac{\pi}{2}\right) = \tau\, R\left(\frac{\pi}{2}\right) = -\frac{\alpha\,\tau}{2}. \tag{5.16}$$

This yields the stability diagram above the dashed diagonal in figure 7. As earlier, the plot is extended below the diagonal by symmetry.

Figure 8 shows typical plots of the function $C_{\rm c}(k, \frac{\pi}{2})$ for various values on the parameters. Again we study the case defined by (5.15). Since the growth rate is plotted for $\theta = \pi/2$, it does not depend on the second flow parameter β, as long as $\beta > \alpha$. Varying the other flow parameter α can drive the system from stable to unstable state. The effect of the relative weight of gravity and surface tension is also illustrated in the figure. Unlike the buckling instability of section 4, this instability produces wrinkles oriented along, and not perpendicular to, the direction achieving largest contraction — which is the x direction with our choice of axes.

The sign of the second derivative of $C_{\rm c}(k, \frac{\pi}{2})$ at $k = 0$ is given by the sign of $[(\gamma_+ - \gamma_-)\,(\rho_1 - 2\rho_2)]$. When $[(\gamma_+ - \gamma_-)\,(\rho_1 - 2\rho_2)] < 0$, the function $C_{\rm c}(k, \frac{\pi}{2})$ has a maximum

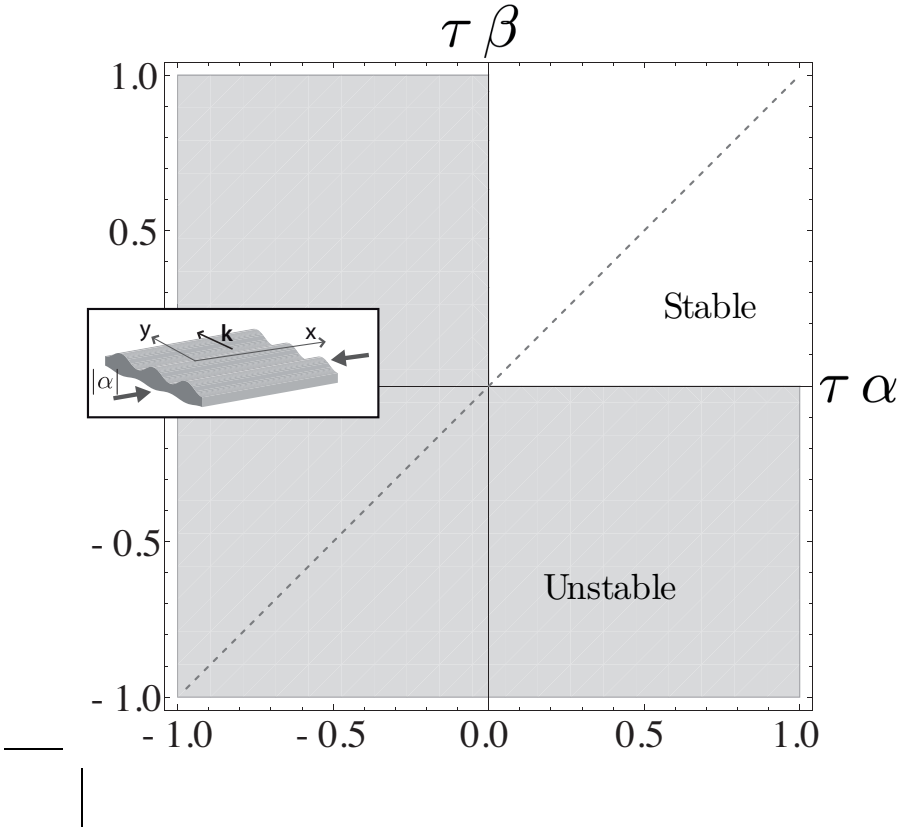

FIGURE 7. Stability with respect to coupled perturbations involving both thickness modulation and deflection of the mid-surface, as determined by the sign of $C_{\rm c}\left(k=0,\theta=\frac{\pi}{2}\right)$ in equation (5.16): phase diagram in the plane of the principal values of strain rate (α,β) rescaled using the time scale τ imposed by gravity and viscosity and defined in (5.10). Equation (5.16) holds above the diagonal ($\alpha<\beta$), the lower part of the diagram being obtained by symmetry.

at $k=0$ and the value of growth factor there determines the stability of the flow:

$$C_{\rm c}^{\max}=C_{\rm c}\left(0,\frac{\pi}{2}\right)=-\frac{1}{2}\left(\alpha+\frac{1}{8\tau}\right)+\frac{\tau}{16\tau_3^2}. \tag{5.17}$$

When $[(\gamma_+-\gamma_-)(\rho_1-2\rho_2)]<0$ and $C_{\rm c}^{\max}>0$, there is a range of unstable wavelengths. Large wavelengths are the most unstable ($k=0$) and as result the instability depends on the details of the boundary conditions at large scale and on the size of the system. This goes beyond the scope of the present analysis, which focuses on local buckling; still, the analysis of these global modes can be performed using the same set of dimensionally reduced equations, taking the appropriate boundary conditions into account.

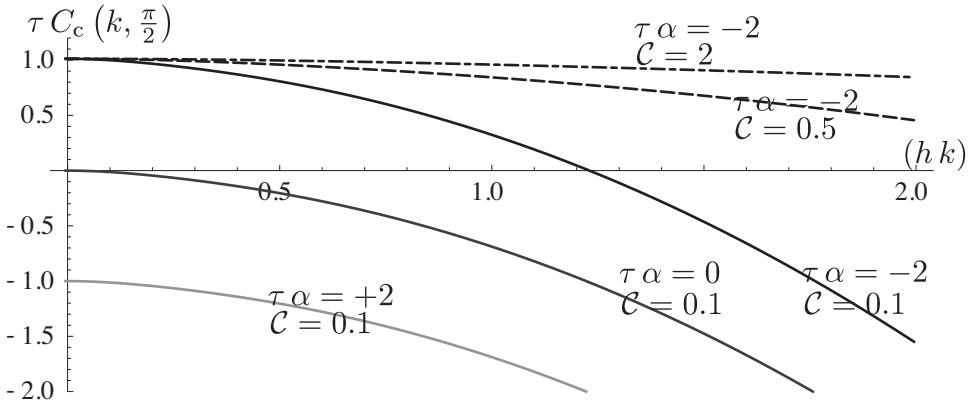

FIGURE 8. Dimensionless growth rate $\tau\, C_c$ for the coupled perturbation, obtained by combining equations (5.14) and (5.15), as a function of the dimensionless wavenumber $h\,k$. Here, τ is a gravity-viscosity timescale, h is the thickness of the sheet, $\mathcal{C}$ is the Bond number defined in (5.10) and α is the most negative (contractile) principal strain rate. The value $\theta = \pi/2$ corresponds to the orientation of the most unstable mode. Note that for this particular value of θ, C_c does not depend on the flow parameter β.

6. Discussion

6.1. *A simplified hybrid model for reconciling the BNT and Trouton buckling analyses*

In Section 4, an undulatory mode of instability has been found to occur using the BNT model. This model is relevant to short times, much shorter than the characteristic time $1/|\alpha| \sim 1/|\beta|$ of the base flow. This buckling mode is made up of stripes perpendicular to the most contractile direction ($\theta = 0$). In the limit of a free-standing viscous sheet, *i. e.* when capillary and buoyancy forces become negligible, this instability occurs whenever $(2\,\alpha + \beta) < 0$, as revealed by setting $\mathcal{C} = 0$ in equation (4.10). By equation (3.13*a*), this corresponds to existence of a compressive membrane stress N^0_{xx} along this most contractile direction x. Then the most unstable mode has infinite wavelength. All these features are characteristic of a buckling instability.

In Section 5, the Trouton model was used. It is based on different scaling assumptions, and in particular is valid for much long times, comparable to $1/|\alpha| \sim 1/|\beta|$. We found a different buckling mode, coupling thickness variations and undulations of the center-surface, and with stripes now parallel to the most contractile direction ($\theta = \pi/2$).

This raises the question of whether these two modes can be in competition, or are a manifestation of a similar phenomenon viewed in two different limits. To answer this question, we propose a hybrid model that reconciles both analyses. This model is formal and simplified, and makes no claims for detailed accuracy. Its only goal is to provide a unified description of the two buckling modes. It is similar to the hybrid model of Section 2.5, with the additional approximation that perturbations to the in-plane flow are neglected. Assuming $\overline{u}_1(x, y, t) = 0$ and $\overline{v}_1(x, y, t) = 0$ for any value of (x, y, t) is consistent with the solution for the undulatory mode and changes quantitatively, but not qualitatively, the behavior of the coupled mode.

Formally, the conservation of mass (3.11) at linear order yields $h_{1,t} + (\alpha + \beta)\, h_1 = 0$. We introduce a growth rate $C = \partial_t$ which is yet unknown, and rewrite this in the hybrid model as:

$$(C + \alpha + \beta)\, \hat{h}_1 = 0. \tag{6.1}$$

We shall soon show that this equation is consistent with the two forms of the conserva-

tion of mass written earlier in the BNT and Trouton buckling analysis, when the two corresponding limits are considered.

We now consider out-of-plane equilibrium. Noting that Trouton form (3.8b) of this equilibrium is a degenerate version of its BNT form (3.8a), we use the latter in the hybrid model. We linearize equation (3.8a) with respect to the perturbation (h_1, H_1). Symbolically, this yields

$$-N_0\, k^2\, \hat{H}_1 = \mu\, {h_0}^3\, C\, k^4\, \hat{H}_1 + (2\, A_2\, \hat{H}_1 + A_1\, \hat{h}_1). \tag{6.2}$$

Here, the coefficient N_0 represents the pre-stress in the base flow, given in equation (3.13), which provides the driving force for the buckling instability. The first term in the right-hand side of equation (6.2) is the bending term. The last term represents the coupling of undulations ($\hat{H}_1$) and thickness variations ($\hat{h}_1$) through buoyancy and surface tension; this coupling is described by the coefficients A_1 and A_2, which have been worked out in the Trouton analysis, see below equation (5.13). Their expressions are similar in the BNT case but we do not need to spell them out here. We shall soon check that the pre-stress and bending terms in equation (6.2) are negligible if the Trouton scaling assumptions are used, as expected.

Equations (6.1) and (6.2) can be combined in matrix form

$$\mathbf{M} \cdot \begin{pmatrix} \hat{h}_1 \\ \hat{H}_1 \end{pmatrix} = \mathbf{0}, \quad \text{where } \mathbf{M} = \begin{pmatrix} C + \alpha + \beta & 0 \\ A_1 & \left(2A_2 + N_0\, k^2 + C\, \mu\, {h_0}^3\, k^4\right) \end{pmatrix}. \tag{6.3}$$

The growth rate is found by requiring that the determinant $\det \mathbf{M} = M_{11}\, M_{22}$ vanishes. One root corresponds to the vanishing of M_{11}, and describes a coupled mode:

$$C = C'_{\mathrm{c}}, \quad \text{where } C'_{\mathrm{c}} = -(\alpha + \beta), \qquad A_1\, \hat{h}_1^{\mathrm{c}} + (2\, A_2 + \cdots)\, \hat{H}_1^{\mathrm{c}} = 0 \tag{6.4a}$$

and the other one to the vanishing of M_{22}, an undulatory mode:

$$C = C'_{\mathrm{u}}, \quad \text{where } C'_{\mathrm{u}} = \frac{1}{(h_0\, k)^2} \left(-\frac{N_0}{\mu\, h_0} - \frac{1}{(h_0\, k)^2}\, \frac{2\, A_2\, h_0}{\mu} \right), \qquad \hat{h}_1 \mathrm{u} = 0. \tag{6.4b}$$

The hybrid model features both a coupled mode and an undulatory mode, and brings the BNT and Trouton analyses under a common framework. Note the close similarity of the expression for $\mathbf{M}$ in equation (6.3) above, with the upper-left block of the matrix $\mathbf{M}$ given earlier in equation (5.13) in the Trouton analysis — the detailed expressions of C_{c} and C'_{c} are different as the hybrid model ignores the perturbation to the in-plane flow. Note also that, formally, the expression (6.4b) for the growth rate C'_{u} of the undulatory mode in the approximate hybrid model, and the expression C_{u} coming from the BNT analysis (4.8) are identical.

From the hybrid model, the Trouton and BNT limits can be recovered by analyzing the orders of magnitude of the growth rates C'_{u} and C'_{c} given above. Let us first introduce the typical time T_{f} associated with the base flow:

$$T_{\mathrm{f}} \sim \alpha^{-1} \sim \beta^{-1} \sim \frac{L}{U}.$$

We use the notations of Section 2 for the orders of magnitude, namely U for in-plane velocity, L for the in-plane length, and ϵ for the aspect ratio h/L. The two growth rates appear to be vastly different:

$$C'_{\mathrm{u}} \sim \frac{N_0}{\mu\, {h_0}^3\, k^2} \sim \frac{\mu\, h_0\, \frac{U}{L}}{\mu\, {h_0}^3\, \frac{1}{L^2}} \sim \frac{1}{\epsilon^2\, T_{\mathrm{f}}}, \qquad C'_{\mathrm{c}} \sim \alpha \sim \beta \sim \frac{1}{T_{\mathrm{f}}}.$$

The typical growth time of the undulatory mode is $1/C'_{\rm u} \sim \epsilon^2\, T_{\rm f}$ is precisely the short time scale of the BNT model ($m = 1$) introduced earlier in equation (2.20a). The typical growth time of the coupled mode is $1/C'_{\rm c} \sim T_{\rm f}$, which is the time scale of the Trouton model ($m = 0$) in equation (2.20a). Stated differently, the coupled perturbation has a vanishing small growth time $C'_{\rm c} = -(\alpha + \beta) \approx 0$ in the BNT framework, meaning that the corresponding mode does not grow significantly over the short time scale $\epsilon^2\, T_{\rm f}$; symmetrically, the undulatory mode is missed in the Trouton analysis as its growth is limited by weak bending stress only: this undulatory mode grows much faster than what the Trouton model can see — when it is actually unstable.

The hybrid model reveals that the two possible unstable modes are actually in competition in a given physical system, even though they were first revealed using two different mathematical models.

If the system is stable with respect to the undulatory mode, the sheet remains flat over the long time scale $T_{\rm f}$. Then, Trouton analysis of buckling applies, and can be used to tell whether a coupled mode develop at long times. Conversely, if the system is unstable with respect to the undulatory mode, the latter grows very rapidly. In this case, the undulatory mode enters into the non-linear regime after a short delay $\sim 1/C_{\rm u} \sim \epsilon^2\, T_{\rm f}$ according to the non-linear analysis of Section 4.2. This is much too early for any coupled perturbation predicted by the analysis of Section 5 to become significant. As a result, the coupled mode may develop with a long delay on top of the undulatory mode, but the analysis presented here is inapplicable as the base state is not planar. We note that the evolution of the two overlapping pattern at long time can not be fully described in an asymptotic study anyway, as can be seen for instance in Smith (1975).

6.2. *Range of validity of the stability analyses*

We now discuss the range of validity of the stability analyses of Section 4 and 5. For simplicity, we restrict ourselves to the case of vanishing surface tension.

For the coupled mode, the characteristic growth time is $T_{\rm f}$, which is also the time scale of the Trouton model. The Jeffreys number takes the form ${\rm Je}_{\rm c} = (\rho\, g\, L\, T_{\rm f})/\mu$, where the wavelength L is generally set by the size of the system. Our assumptions require ${\rm Je}_{\rm c} \gg 1$, which can be achieved, for instance, if the size L of the system is large enough.

For the undulatory (buckling) mode, the characteristic time for growth is $(z^*/L)^2\, T_{\rm f}$, consistent with the choice of the BNT scaling. It grows at a much faster rate than the coupled mode, as the aspect ratio (z^*/L) is small. Using the scaling $[(\rho\, g\, T_{\rm f})/(z^*\mu)]^{1/2}$ found for the wavelength of the most unstable mode in equation (4.12), Jeffreys number reads ${\rm Je}_{\rm u} = [(\rho\, g\, h\, T_{\rm f})/\mu]^{1/2}$. Our assumptions require ${\rm Je}_{\rm u} \ll 1$, which can be achieved if, for instance, the thickness is small enough.

The validity of our analyses for the buckling and coupled instabilities require ${\rm Je}_{\rm c} \gg 1$ and ${\rm Je}_{\rm u} \ll 1$, respectively. We note that these conditions are not mutually exclusive. Both can be met if $h \ll \frac{\mu}{\rho g\, T_{\rm f}} \ll L$. In such circumstances, both instabilities can be observed concurrently, keeping in mind the limitations mentioned at the end of Section 6.1.

6.3. *Orders of magnitude*

We compute here some orders of magnitude for the two modes in the cases of compressional tectonics of the Earth's crust and plate glass production. In the two applications, the bath is much less viscous than the two sheets. For the earth crust floating on the upper mantle we use the following values: $h = 10$ km, $L = 1000$ km, $\mu = 10^{23}$ kg.m^{-1}.s^{-1}, $\alpha = -10^{-14}$ s^{-1}, $\rho_1 = 2800$ kg.m^{-3}, $\rho_2 = 3400$ kg.m^{-3} and $\gamma_+ = \gamma_- = 0$ N.m^{-1}. These values are only indicative: the rheology of geophysical fluids is non-Newtonian, while the geometry and the loading are complex. For a glass sheet floating on molten

tin, we use the following parameters: $h = 3$ mm, $\mu = 10^5$ kg.m^{-1}.s^{-1}, $\alpha = -0.03$ s^{-1}, $\rho_1 = 2500$ kg.m^{-3}, $\rho_2 = 6500$ kg.m^{-3} and $\gamma_+ + \gamma_- = 1$ N.m^{-1}. Note that the viscosity of glass is highly dependent on temperature, which may impact on the orders of magnitude obtained below. This yields the following orders of magnitude for the Jeffreys number:

$$\mathrm{Je_c} \approx 30, \quad \mathrm{Je_u} \approx 5 \cdot 10^{-1} \text{ (earth crust)}, \qquad \mathrm{Je_c} \approx 10^2, \quad \mathrm{Je_u} \approx 10^{-1} \text{ (molten glass)}. \tag{6.5}$$

The values of the Jeffreys number are not always asymptotic and the corresponding predictions are only qualitative. For the undulatory (buckling) mode, the typical growth time $\tau = 1/C_\mathrm{c}^\mathrm{max}$ and wavelength $\lambda = 1/k_\mathrm{max}$ are given by equation (4.12). In the earth application, this yields a wavelength of about 150 km and a typical time of 100 000 years. Our non-linear analysis predicts an amplitude of deformation of about $h = 10$ km in the same typical time. The lengthscales are satisfying while the time scale is an order of magnitude too small. This might be ascribed to the various simplifications of the problem. In the glass application, we obtain a wavelength of several centimeters $\lambda \approx 10$ cm and a typical time $\tau \approx 10^{-1}$ s. The non-linear analysis predicts that the amplitude of deformation reaches the thickness of the glass sheet in this typical time. The wavelength matches the typical wavelengths of imperfections observed on float glass, and correctly predicts the orientation of stripes perpendicular to the direction of stretching (buckling mode). However, we cannot predict the amplitude because the process is intrinsically nonstationary: the flow is compressive and extensional according to the position along the bath.

The coupled mode is more unstable for small wavenumbers. As a result, its wavelength and direction are controlled by the geometry of the system at large scale. We shall only estimate the typical growth time $\tau = 1/C_\mathrm{c}^\mathrm{max}$ where $C_\mathrm{c}^\mathrm{max}$ from equations (5.17). In the earth application the typical growth time is 6 million years, which is a sensible geological time scale. This mode might correspond to the variable thickness of the crust across mountain ranges. In the glass application, the typical growth time is 10^2 s which is comparable to the typical residence time of the glass in the float process, which could explain the large scale imperfections of the thickness of float glass.

6.4. *Conclusion*

We have derived a reduced, 2D model for thin viscous sheets subjected to arbitrary forces applied in the bulk or on the interfaces. The equations are compact, and expressed in terms of thickness-averaged quantities such as position, velocity, in-plane stress and bending moments. Such formulations have been extensively used for elastic plates and shells, but have received much less attention in the context of viscous sheets. Our equations are valid for weak deflections from a straight configuration, and are well suited to the analysis of buckling. The models based on the Trouton and BNT scalings were derived in a unified manner. We presented a comprehensive analysis of the buckling of thin floating sheets for arbitrary base flows. A planar base flow can become unstable when it induces a large enough contraction along some tangent direction. We identified a buckling mode with a wavenumber aligned with the direction of most vigorous contraction, and a coupled mode with a wavenumber perpendicular to it it. In addition, the non-linear evolution of buckling was studied, revealing a cross-over between the short-time, exponential evolution of the amplitude, as predicted by linear stability, to a large-time, square-root evolution of the amplitude, as imposed by kinematics. The equations for thin viscous sheets subjected to external forces derived in this paper provide a framework applicable to a variety of problems and geometries, and can serve as a basis for an efficient numerical implementation.

We would like to thank Paul Clavin and Jean-Marc Chomaz for suggesting useful bibliographical references. Careful reviews by Neil Ribe and two anonymous referees were extremely useful for the improvement of the initial manuscript.

Appendix A. Identities for slice-based operators

Taking the derivative with respect to x of the definition (2.3a) for the thickness-integral operator I, we have for a fixed time

$$[I\cdot(\phi_{,x})](x) = \frac{\mathrm{d}[I\cdot\phi]}{\mathrm{d}x} - \phi(x,z_+(x))\,\frac{\mathrm{d}z_+}{\mathrm{d}x} + \phi(x,z_-(x))\,\frac{\mathrm{d}z_-}{\mathrm{d}x}. \tag{A 1}$$

The two last term come from the fact that the interval of integration, $z_-(x)\le z\le z_+(x)$, has non-constant endpoints. We refer to this formula as 'integration by parts along the z direction'.

When the argument of the operator I is an exact derivative with respect to z, we can carry out the integration explicitly:

$$[I\cdot(\phi_{,z})](x) = \phi(x,z_+(x)) - \phi(x,z_-(x)). \tag{A 2}$$

These identities can be turned into identities for the first-moment operator J by a special choice of the function ϕ:

$$\phi(x,z) = (z-H(x))\,\gamma(x,z)$$

for some function $\gamma(x,z)$. For that particular choice of ϕ, the definition (2.3b) of J reads:

$$[I\cdot\phi](x) = [J\cdot\gamma](x).$$

Substituting into the first identity (A 1), we have

$$[I\cdot(-H_{,x}\,\gamma)](x) + [J\cdot(\gamma_{,x})](x) = \frac{\mathrm{d}[J\cdot\gamma]}{\mathrm{d}x} - \frac{h(x)}{2}\,\left(z_{+,x}(x)\,\gamma_+(x) + z_{-,x}(x)\,\gamma_-(x)\right), \tag{A 3}$$

where $\gamma_\pm(x)$ is a shorthand notation for $\gamma(x,z_\pm(x))$.

Substituting into the second identity (A 2), we find

$$[I\cdot\gamma](x) + [J\cdot(\gamma_{,z})] = \frac{h(x)}{2}\,\left(\gamma_+(x)+\gamma_-(x)\right). \tag{A 4}$$

Another identity follows from the definitions (2.3d) and (2.3e) of the operators A and χ:

$$[\chi\cdot\phi](x) = \frac{1}{2}\,\Big([A\cdot\phi](x,z_+(x)) + [A\cdot\phi](x,z_-(x))\Big). \tag{A 5}$$

A last set of identities allows one to rewrite the composition of the operator A with either I or J in terms of the first and second moments J or K:

$$[I\cdot[A\cdot\phi]](x) = h(x)\,[\chi\cdot\phi](x) - [J\cdot\phi](x), \tag{A 6a}$$

$$[J\cdot[A\cdot\phi]](x) = \frac{h^2(x)}{8}\,[I\cdot\phi](x) - [K\cdot\phi](x). \tag{A 6b}$$

These identities follow from a permutation of the two integrals associated with the operators in the left-hand sides. The most direct proof is to notice that both sides of each equality are linear forms of ϕ, and to check the equalities when ϕ is a Dirac function, $\phi(z)=\delta_D(z-z_0)$, studying the cases $z_-<z_0<H$ and $H<z_0<z_+$ separately. Details of the proof are left to the reader.

Appendix B. Interpretation of the equations of equilibrium

Here, we propose an interpretation of the equations (2.11) and (2.15) for the equilibrium of a thin 2D sheet, by showing equivalence with the Kirchhoff equations for a thin rod. The equations of equilibrium (2.32) and (2.33*b*) in a 3D geometry have a similar structure, and can be interpreted similarly.

In a thin elastic rod, the resultant and moment of internal stress $\mathbf{S}$ over a cross-section are noted $\mathbf{n}(x)$ and $\mathbf{m}(x)$, and the balance of force and moment over a small length of the rod is expressed by the classical Kirchhoff equations:

$$\mathbf{n}'(x) + \mathbf{p}(x) = \mathbf{0} \tag{B 1}$$

$$\mathbf{m}'(x) + \mathbf{t}(x) \times \mathbf{n}(x) + \mathbf{q}(x) = \mathbf{0}. \tag{B 2}$$

With the right-hand sides set to zero, this defines the equations of equilibrium. Here, $\mathbf{p}(x)$ and $\mathbf{q}(x)$ are the lineic densities of applied forces and moments, and $\mathbf{t}(x)$ is the tangent to the centerline.

We are concerned with a 2D geometry, restricted to the (x, z) plane: $\mathbf{n} = (n_x, 0, n_z)$, $\mathbf{m} = (0, m_y, 0)$, $\mathbf{p} = (p_x, 0, p_z)$, $\mathbf{q} = (0, q_y, 0)$. In addition, we consider the small slope approximation: $\mathbf{t} = (1, 0, H_{,x})$, the quantity $H_{,x}$ being small, of order ϵ. Projection of Kirchhoff equations onto the axes yields:

$$n_{x,x} + p_x = 0 \tag{B 3}$$

$$n_{z,x} + p_z = 0 \tag{B 4}$$

$$m_{y,x} - n_z + H_{,x}\, n_x + q_y = 0. \tag{B 5}$$

Elimination of the normal internal force n_z by equation (B 5) and substitution into equation (B 4) yields:

$$m_{y,xx} + (H_{,x}\, n_x)_{,x} + q_{y,x} + p_z = 0. \tag{B 6}$$

We can identify the axial balances of forces (2.11) and (B 3) on one hand, and the transverse balances of forces (2.15) and (B 6) on the other hand with the following variables:

$$n_x = N_{xx} \tag{B 7}$$

$$m_y = M_{xx} \tag{B 8}$$

$$p_x = [I \cdot f_x^{(0)}] \tag{B 9}$$

$$p_z = [I \cdot f_z^{(1)}] \tag{B 10}$$

$$q_y = [J \cdot f_x^{(0)}] \tag{B 11}$$

REFERENCES

Barnes, G. & Woodcock, R. 1958 Liquid rope-coil effect. *Am. J. Phys.* **26** (205-209).

Benjamin, T. B. & Mullin, T. 1988 Buckling instabilities in layers of viscous liquid subjected to shearing. *J. Fluid Mech.* **195**, 523–540.

Biot, M. A. 1964 Theory of viscous buckling of multilayered fluids undergoing finite strain. *Phys. Fluids* **7**, 855–861.

Blake, K. R. & Bejan, A. 1984 Experiments on the buckling of thin fluid layers undergoing end-compression. *J. Fluids Eng.* **106**, 74–78.

Boudaoud, A. & Chaïeb, S. 2001 Singular thin viscous sheet. *Phys. Rev. E* **64**, 050601.

Buckmaster, J. D. & Nachman, A. 1978 The buckling and stretching of a viscida II. effects of surface tension. *Q. J. Mech. Appl. Math.* **31**, 157–168.

Buckmaster, J. D., Nachman, A. & Ting, L. 1975 The buckling and stretching of a viscida. *J. Fluid. Mech.* **69**, 1–20.

Charru, F. 2007 *Instabilités hydrodynamiques*. CNRS Edition.

Ciarlet, Ph. G. 1980 A justification of the von Kármán equations. *Archive for Rational Mechanics and Analysis* **73** (4), 349–389.

Cruickshank, J. O. & Munson, B. R. 1982 A theoretical prediction of the fluid buckling frequency. *Phys. Fluids* **25**, 1935–1937.

Da Silveira, R., Chaïeb, S. & Mahadevan, L. 2000 Rippling instability of a collapsing bubble. *Science* **287** (5457), 1468–1471.

Debrégeas, G., de Gennes, P. G. & Brochard-Wyart, F. 1998 The life and death of "bare" viscous bubbles. *Science* **279** (5357), 1704–1707.

Dret, H. Le & Raoult, A. 1995 The nonlinear membrane model as variational limit of three-dimensional nonlinear elasticity. *Journal de Mathématiques Pures et Appliquées* **75**, 551–580.

Dyson, R. J. & Jensen, O. E. 2010 A fibre-reinforced fluid model of anisotropic plant cell growth. *J. Fluid Mech.* **655**, 472–503.

England, P. & McKenzie, D. 1983 Correction to: a thin viscous sheet model for continental deformation. *Geophys. J. R. astr. Soc.* **73** (523-532).

Filippov, A. & Zheng, Z. 2010 Dynamics and shape instability of thin viscous sheets. *Physics of Fluids* **22** (023601).

Griffiths, I. M. & Howell, P. D. 2007 The surface-tension-driven evolution of a two-dimensional annular viscous tube. *Journal of Fluid Mechanics* **593**, 181–208.

Griffiths, I. M. & Howell, P. D. 2008 Mathematical modelling of non-axisymmetric capillary tube drawing. *J. Fluid Mech.* **605**, 181–206.

Griffiths, I. M. & Howell, P. D. 2009 The surface-tension-driven retraction of a viscida. *SIAM J. Appl. Math.* **70** (5), 1453–1487.

Guillou-Frottier, L, Buttles, J & Olson, P 1995 Laboratory experiments on the structure of subducted lithosphere. *Earth Planet. Sci. Lett.* **133**, 19–34.

Howell, P. D. 1996 Models for thin viscous sheets. *Eur. J. Appl. Math.* **7**, 321–343.

Jeffreys, H. 1925 The flow of water in an included channel of rectangular section. *Philosophical Magazine* **49** (793).

Johnson, A M & Fletcher, R C 1994 *Folding of viscous layers: mechanical analysis and interpretation of structures in deformed rock*. Columbia Univ. Press.

Kücken, M. & Newell, A. C. 2004 A model for fingerprint formation. *Europhys. Lett.* **68**, 141–146.

Lifschitz, A. & Hameiri, E. 1991 Local stability conditions in fluid dynamics. *Physics of Fluids A: Fluid Dynamics* **3** (11), 2644.

Mahadevan, L., Ryu, S. & Samuel, A. D. T. 1998 Fluid rope trick investigated. *Nature* **392**, 140.

Manneville, P. 2004 *Instabilities, chaos and turbulence*. Imperial College Press.

Marheineke, N & Wegener, R 2009 Asymptotic model for the dynamics of curved viscous fibres with surface tension. *J. Fluid Mech.* **622**, 345–369.

O'Keefe, J. A. 1969 Water on the moon and a new nondimensional number. *Science* **163**, 669.

Pearson, J. R. A. 1985 *Mechanics of Polymer Processing*. Elsevier.

Pearson, J. R. A. & Petrie, C. J. S. 1970*a* The flow of a tubular film. part 1. formal mathematical representation. *J. Fluid Mech.* **40** (1), 1–19.

Pearson, J. R. A. & Petrie, C. J. S. 1970*b* The flow of a tubular film. part 2. interpretation of the model and discussion of solutions. *J. Fluid Mech.* **42** (3), 609–625.

Perazzo, Carlos Alberto & Gratton, Julio 2010 Convergent flow in a two-layer system and mountain building. *Phys. Fluids* **22** (056603).

Pfingstag, G., Audoly, B. & Boudaoud, A. 2011 Thin viscous sheets with inhomogeneous viscosity. Submitted to Phys. Fluids.

Pilkington, A. 1969 The float glass process. *Proceedings of the Royal Society of London A.* **314**, 1–25.

Ramberg, H. 1981 *Gravity, Deformation and the Earth's Crust*, 2nd edn. Academic Press, London.

Rayleigh, J. W. 1896 *The Theory of Sound*. London: Macmillan.

Ribe, N. M. 2001 Bending and stretching of thin viscous sheets. *J. Fluid Mech.* **433**, 135–160.

Ribe, N. M. 2002 A general thoery for the dynamics of thin viscous sheets. *J. Fluid Mech.* **457**, 255–283.

Ribe, N M, Stutzmann, E, Ren, Y & van der Hilst, R 2007 Buckling instabilities of subducted lithosphere beneath the transition zone. *Earth Planet. Sci. Lett.* **254**, 173–179.

Scheid, B., Quiligotti, S., Tran, B. & Stone, H. A. 2009 Lateral shaping and stability of a stretching viscous sheet. *The European Physical Journal B* .

Smith, R. B. 1975 Unified theory of the onset of folding, boudinage, and mullion structure. *Geological Society of America Bulletin* **86**, 1601–1609.

Steele, C. R. 2000 Shell stability related to pattern formation in plants. *Journal of Applied Mechanics* **67** (2), 237.

Stokes, G. G. 1845 On the theories of the internal friction of fluids in motion and of the equilibrium and motion of elastic solids. *Trans. Cambridge Phil. Soc.* **8**, 287, in Mathematical and Physical Papers.

Suleiman, S. M. & Munson, B. R. 1981 Viscous buckling of thin fluid layers. *Phys. Fluids* **24**, 1–5.

Taylor, G. I. 1968 Instabilities of jets, threads and sheets of viscous fluid. In *Proceedings of the 12th International Congress of Applied Mechanics* (ed. Springer-Verlag), pp. 382–388. Stanford.

Toro, R. & Burnod, Y. 2005 A morphogenetic model for the development of cortical convolutions. *Cereb. Cortex* pp. 1900–1913.

van de Fliert, B. W., Howell, P. D. & Ockendon, J. R. 1995 Pressure-driven flow of a thin viscous sheet. *J. Fluid Mech.* **292**, 359–376.

Yarin, A. L., Gospodinov, P. & Roussinov, V. I. 1994 Stability loss and sensitivity in hollow fiber drawing. *Physics of Fluids* **6** (4).

Zel'dovich, Ya. B., Istratov, A. G., Kidin, N. I. & Librovich, V. B. 1980 Flame propagation in tubes: hydrodynamics and stability. *Combustion science and technology* **24** (1–2), 1–13.